ELSEVIER

Contents lists available at ScienceDirect

Journal of Hydrology

journal homepage: www.elsevier.com/locate/jhydrol



Research papers

A Bayesian adaptive reservoir operation framework incorporating streamflow non-stationarity

Guang Yang ^a, Benjamin Zaitchik ^b, Hamada Badr ^b, Paul Block ^{a,*}

- ^a Department of Civil and Environmental Engineering, University of Wisconsin-Madison, 1415 Engineering Dr., Madison, WI 53706, USA
- ^b Department of Earth and Planetary Sciences, The Johns Hopkins University, Baltimore, MD, USA



This manuscript was handled by Sally Elizabeth Thompson, Editor-in-Chief, with the assistance of Newsha Ajami, Associate Editor

Keywords: Adaptive reservoir operation Reservoir operating rules Streamflow non-stationarity Bayesian model average Time-frequency analysis

ABSTRACT

Water reservoir operating rules are typically derived based on the assumption of streamflow stationarity, however, this assumption could be undermined by climate change. Adaptive reservoir operation is one of the most effective strategies to support water resources management under non-stationarity, yet until now, adaptive strategies considering non-stationarity across multiple time scales are rarely investigated. We propose an adaptive reservoir operation framework that incorporates streamflow non-stationarity across time scales simultaneously. Specifically, we first decompose the streamflow into four frequency categories to detect nonstationarity features through reservoir operation simulations. Next, we incorporate the non-stationarity information from each frequency category into adaptive reservoir operation by using Bayesian Model Averaging. We apply this framework to reservoir operation of the Grand Ethiopian Renaissance Dam on the Blue Nile River and evaluate its effectiveness with streamflow simulated from 21 general circulation models (GCMs) for two greenhouse gases emission scenarios. We find that streamflow non-stationarity from all GCMs varies by future period and frequency category. The proposed Bayesian adaptive reservoir operation framework can detect streamflow non-stationarity across all frequency categories and predominantly outperforms conventional adaptive strategies, especially in terms of firm power output. In general, firm output increases under the Bayesian framework as the power generation reliability increases. The proposed framework offers a robust approach to identify adaptive strategies for reservoir operation to address streamflow non-stationarity.

1. Introduction

Rapid socio-economic development, population growth, and changes in preferences and consumption patterns continue to propel increasing global water demand (WWAP, 2019). Concurrently, climate change is likely to alter water supply availability, given expected changes to the hydrologic cycle, including precipitation, temperature, and streamflow, challenging water resources management (Allen and Ingram, 2002; Gosling and Arnell, 2016; Milly et al., 2005; Poff et al., 2016). Surfacewater reservoirs are effective infrastructure means to reallocate water resources spatially and temporally to address sectoral conflicts between agriculture, power generation, water supply, tourism, etc. (Gaudard et al., 2014), however as stressors on water demand and supply accelerate, novel methods to improve reservoir management and efficiency are becoming increasingly valuable (Giuliani et al., 2016; Gleick, 2003).

In recent decades, strategies to improve reservoir operations have been widely investigated, including those based on neural networks algorithms, e.g. (Cancelliere et al., 2002; Chaves and Chang, 2008), genetic programming, e.g. (Ashofteh et al., 2015; Xiong et al., 2019), adaptive neural fuzzy inference systems, e.g. (Soltani et al., 2010), decision tree algorithms, e.g. (Herman and Giuliani, 2018; Yang et al., 2016), and others. Although these methods have demonstrated improved effectiveness and efficiency in reservoir operations, they are traditionally applied based on the assumption of future hydrologic stationarity. Given expected future large-scale changes to the global climate system (Culley et al., 2016; Milly et al., 2008), statistical properties (e.g., expected value, variance, and coefficient of variation) of hydrologic variables could change with time and be a deterministic function of time (described as non-stationarity (Koutsoyiannis and Montanari, 2015)) and this assumption could be problematic. Because of hydrologic non-stationarity, the statistical properties of reservoir inflow in the future could be different from historical levels. In this way, the reservoir operating rules optimized from observed streamflow data may not be suitable for reservoir decision-making in the future.

E-mail addresses: gyang82@wisc.edu (G. Yang), pblock2@wisc.edu (P. Block).

^{*} Corresponding author.

To address this, adaptive reservoir operation models have been developed, modified and applied to assess the impacts of climate change and support long-term reservoir operation strategies (Ahmadi et al., 2015; Block and Strzepek, 2010; Borgomeo et al., 2014; Brown et al., 2015; Chang et al., 2018; Culley et al., 2016; Ehsani et al., 2017; Herman et al., 2015; Jeuland and Whittington, 2014; Maier et al., 2016; Steinschneider and Brown, 2012; Walsh et al., 2016; Xu et al., 2014). For example, Xu et al. (2014) propose reservoir hedging rules adaptive to non-stationary inflow conditions based on an autoregressive integrated moving average model. Borgomeo et al. (2014) develop a risk-based decision-making framework for long-term reservoir operations under climate change by incorporating non-stationary probabilistic climate projections obtained from a stochastic weather generator. Ahmadi et al. (2015) simulate reservoir inflows based on hydrologic conditions from global general circulation models to derive reservoir operating rules for power generation under climate change. Culley et al. (2016) design reservoir operating rules adaptive to climate change by using a bottomup approach (Brown et al., 2012) and evaluate the upper limit of adaptive capacity in reservoir operations. The adaptive reservoir operation framework here is also noted as "dynamic planning" or "dynamic adaptive plan" in some literatures (Haasnoot et al., 2013; Herman et al., 2019).

In adaptive framework, detection-based and simulation-based approaches are typically used to overcome the hydrologic non-stationarity and improve the adaptivity of reservoir operating rules. Detection-based approaches first determine the presence of non-stationarity (e.g. by analyzing historical streamflow directly or detecting trends in the impacts of thermodynamic climate change, such as snowpack decline (Ceres et al., 2017) and sea level rise (Thorarinsdottir et al., 2017)), and subsequently generate synthetic streamflow considering detected nonstationarity features (such as a trend) in historical streamflow to derive reservoir operating rules (Xu et al., 2014). Recently, signposts or triggers for non-stationarity detection have been investigated to determine "when to adapt" in water resources operation and planning (Fletcher et al., 2019; Raso et al., 2019; Robinson and Herman, 2019). Simulation-based approaches do not rely on non-stationarity detection but rather determine reservoir operating rules based on streamflow simulated from future climate projections (Chang et al., 2018; Culley et al., 2016; Haasnoot et al., 2013; Ngo et al., 2018). For example, the representative concentration pathways (RCPs) developed in the fifth assessment report of the Intergovernmental Panel on Climate Change (IPCC) (Taylor et al., 2012) have been used to project climate scenarios. Subsequently, streamflow simulated from the climate scenarios (of precipitation, temperature, etc.) using a hydrological model is used to derive reservoir operating rules.

For both approaches, reservoir operating rules are derived from synthetic or projected streamflow time series directly and only the impact of possible streamflow non-stationarity at specific time scale is considered (e.g., the reservoir operating rules derived from monthly projected streamflow data typically only consider non-stationarity at a monthly scale). However, changes in climate may cause changes in streamflow variability at different time-scale (Katz and Brown, 1992), potentially affecting reservoir operations uniquely. For example, longterm variability (low-frequency information) in streamflow typically has less impact than short-term variability (high-frequency information) on reservoir operations for flood control (Herman and Giuliani, 2018). Also, both the degree and the source of non-stationarity in streamflow can vary at multiple timescales, which indicates that the adaptive reservoir operating rules considering the impact of multiple timescale non-stationarity need to be dynamic. For example, a dynamic reservoir operation strategy based on rolling decision procedure (i.e., recalibrating reservoir operating rules every 5-10 years) (Xu et al., 2014) can be used to enhance the robustness to streamflow non-stationarity (Yang and Ng, 2017).

In recent years, model merging techniques such as Bayesian Model Averaging (BMA), which have been widely applied in hydrologic

predictions (Diks and Vrugt, 2010; Duan et al., 2007; Huang et al., 2019; Rathinasamy et al., 2013; Zhang et al., 2009), are also used in reservoir operations (Koppa et al., 2019; Yang et al., 2020; Zhang et al., 2015). The BMA method is able to provide less risky inferences or estimations (Hoeting et al., 1999) by combining multiple models, which can be also used to improve reservoir decision making. For example, Zhang et al. (2015) combine three individual reservoir operation models with BMA and find this method can reduce the uncertainty of reservoir operating rules. To consider streamflow non-stationarity at multiple time scales simultaneously in reservoir decision-making, we develop a Bayesianbased adaptive reservoir operation framework using the BMA method. Specifically, we (1) decompose streamflow time series into multiple frequency categories (e.g., high, median, and low frequency information, representing seasonal, annual, and multi-year streamflow variability, respectively), (2) evaluate their impacts on the robustness of reservoir operating rules (to recognize the sources of non-stationarity related to reservoir operation, e.g., if the median frequency information has the greatest impact, the non-stationarity at annual scale is assumed most significant), and (3) merge the impacts of non-stationarity of different frequency categories into reservoir decision making using Bayesian Model Averaging.

We select the Grand Ethiopian Renaissance Dam (GERD) on the Blue Nile River in Ethiopia to demonstrate the framework and provide quantitative analysis. As in simulation-based approaches, we simulate GERD reservoir inflow series in the future from Global Climate Models (GCMs) under a suite of representative concentration pathways developed in the fifth assessment report of IPCC (Taylor et al., 2012) to evaluate the performance of our adaptive reservoir operation framework. It is worth noting that we are not using the simulated streamflow to provide "accurate" projections of future conditions at GERD, but to enhance the understanding of GERD reservoir operation under non-stationary conditions.

This work contributes to an improved understanding of how possible non-stationarity in streamflow may affect conventional water resources operations and provides a creative way to detect the impacts of non-stationarity on reservoir operations and modify existing reservoir operating rules.

2. Study area and data

2.1. The Blue Nile basin and the Grand Ethiopian Renaissance Dam

The Blue Nile River, the most significant tributary of the Nile River, originates at Tana Lake in Ethiopia and merges with the White Nile River in Khartoum, Sudan. Average annual rainfall in the upper part of the basin varies between 1200 and 1800 mm (Conway, 2000), with a dominant rainy season in June–September contributing approximately 70% of mean annual precipitation. During this season, the Blue Nile supplies nearly 80% of total Nile River streamflow, on average, vital to livelihood and development in Ethiopia, Sudan and Egypt.

The GERD, situated on the Blue Nile River in western Ethiopia approximately 15 km upstream of the Sudanese border and currently under construction, will become the largest hydroelectric dam in Africa (King and Block, 2014). When completed, the GERD will have a reservoir capacity of 74 billion cubic meters, a rated power capacity of 6,000 MW, and produce an average of 15,130 GWh of electricity annually, nearly tripling Ethiopia's current production (Tesfa, 2013). With electricity demand in Ethiopia projected to grow at a rate of approximately 30% per year (ETHIOPIA: Power Sector Market, 2016) the GERD is expected to contribute to both Ethiopia's national energy grid as well as benefit other countries in the East African power pool (Nile Basin Initiative, 2012). Ethiopia's 15-year Growth and Transformation Plan (National Planning Commission, 2016) outlines a strategy to reach middle-income country status by 2025; development of the GERD is a major centerpiece of this plan.

2.2. Streamflow data and climate change projections

2.2.1. Historical analysis

A daily record of Blue Nile River flow data was obtained for the El Diem gauging station, located just downstream of the GERD site, and averaged to monthly flow estimates. As the El Diem record is only available through 2009 and contains significant gaps, we performed a hydrological simulation of the Blue Nile basin using the Noah Land Surface Model (Noah LSM) (Ek et al., 2003) paired with the Hydrological Mapping and Analysis Platform (Getirana et al., 2012), implemented with the NASA Land Information System (Kumar et al., 2006), to supplement the historical record. These simulations were implemented at a 10 km horizontal resolution for the period 1981-2016 and use meteorological forcing from the NASA Modern Era Reanalysis for Research and Applications, version 2 (MERRA-2) (Gelaro et al., 2017), but with precipitation drawn from the Climate Hazards InfraRed Precipitation with Stations, version 2 (CHIRPSv2) (Funk et al., 2015) satellite-informed product. Monthly river flow estimates at the GERD site were bias corrected conditioned on the overlapping period with the El Diem gauge record. This record was compared to an independently collected streamflow record from the GERD site for 1954 to 2003, and agreement is strong (Nash-Sutcliffe Efficiency (Nash, 1970) of 0.76) for the common period.

The minimum daily temperature, maximum daily temperature, and precipitation forcing data used in the Noah LSM simulations—MERRA-2 temperature and CHIRPSv2 precipitation—were extracted as basin-wide monthly averages and used to train an artificial neural network (ANN) model to predict streamflow at the GERD site as a function of precipitation and temperature. The ANN was implemented using the nnetar function from the "forecast" R package (Hyndman and Khandakar, 2007). It fits a single-hidden-layer feed-forward ANN with lagged inputs to predict log transformation of GERD streamflow as a function of meteorological predictors. The model was trained to capture the relationship between GERD streamflow and different combinations of predictors including autoregression (timeseries forecasting, no predictors), precipitation volume for the watershed area, and air temperature. The model parameters (network size and weight decay) are tuned based on the ANN results from Badr et al. (2014) and the output from the ANN is used as the historical streamflow.

2.2.2. Streamflow based on climate change projections

To project future Blue Nile River flow at the GERD site, we applied the ANN using temperature and precipitation fields extracted from the NASA Earth Exchange Global Daily Downscaled Projections (NEX-GDDP; (Thrasher et al., 2013)). The NEX-GDDP meteorological fields are 0.25° resolution gridded fields generated through a bias correction and statistical disaggregation of selected Global Climate Model (GCM) outputs from the 5th Coupled Model Intercomparison Project (CMIP5) (Taylor et al., 2012). Since NEX-GDDP is bias corrected to a different meteorological reference from the one used in our study, we performed an additional simple bias correction to provide consistency with our historical record. NEX-GDDP includes output for single runs from 21 CMIP5 GCMs (Table 1) for the historical simulations (through 2005) and for two projections—the high emissions Representative Concentration Pathway 8.5 (RCP8.5) (Moss et al., 2010) and moderate emissions RCP4.5—for the period 2006-2100. The NEX-GDDP projections for precipitation and temperature extend beyond the historically observed range of these variables, as expected under future climate conditions. The predicted precipitation fields also appear to be unrealistic for some GCMs, particularly for RCP8.5 in the second half of the 21st century. This is not uncommon for local to regional scale precipitation projections in GCMs. As the focus of this paper is to understand reservoir operation under non-stationary conditions, rather than to present specific predictions for future GERD observations, we do not perform GCM selection or weighting to optimize realism of future projections Fig. 1.

Historical data (1954 to 2003) at the GERD site illustrate expected

Table 1
List of 21 CMIP5 climate models used for analyzing future climate change for Blue Nile.

ID	ID Model Modeling Centre/Institution abbreviation				
1	ACCESS1-0	ommonwealth Scientific and Industrial Research rganization (CSIRO) and Bureau of Meteorology (BOM), ustralia			
2	BCC-CSM1-1	Beijing Climate Center, China Meteorological Administration, China			
3	BNU-ESM	College of Global Change and Earth System Science, Beijing Normal University, China			
4	CanESM2	Canadian Centre for Climate Modeling and Analysis, Canada			
5	CCSM4	University of Miami - RSMAS, United States			
6	CESM1-BGC	Community Earth System Model Contributors, NSF–DOE–NCAR, United States			
7	CNRM-CM5	Centre National de Recherches Météorologiques, France			
8	CSIRO-Mk3-6-0	CSIRO - Queensland Climate Change Centre of Excellence, Australia			
9	GFDL-CM3	NOAA Geophysical Fluid Dynamics Laboratory, United			
10	GFDL-ESM2G	States			
11	GFDL-ESM2M				
12	INM-CM4	Institute for Numerical Mathematics, Russia			
13	IPSL-CM5A-LR	Institute Pierre-Simon Laplace, France			
14	IPSL-CM5A-MR				
15	MIROC5	Japan Agency for Marine-Earth Science and Technology,			
16	MIROC-ESM	Atmosphere and Ocean Research Institute, and National			
17	MIROC-ESM- CHEM	Institute for Environmental Studies, Japan			
18	MPI-ESM-LR	Max Planck Institute for Meteorology, Germany			
19	MPI-ESM-MR	Max Planck Institute for Meteorology, Germany			
20	MRI-CGCM3	Meteorological Research Institute, Japan			
21	NorESM1-M	Norwegian Climate Centre, Norway			

high reservoir inflows in July to October and comparatively low inflow in the remaining months (Fig. 2.) Considering climate change scenario RCP4.5, median reservoir inflow for all 21 GCMs in the future is similar to historical inflow, especially for June to August, however for scenario RCP8.5, their difference becomes evident (Fig. 2.) Both scenarios project higher annual inflow volumes, with the increase mainly occurring during the peak flow season. For example, the GCM median of August and September inflow during 2071–2100 is projected to be almost twice the historical inflow. Additionally, inflow uncertainty is also highest during this season, and particularly notable for RCP8.5 (Fig. 2(b).) In this study, the inflow data simulated from the two RCP scenarios are used in reservoir operation simulations, which enables examining the adaptivity of the proposed reservoir operation framework under various streamflow patterns.

3. Models and methods

3.1. Reservoir operation model

Hydropower production is the primary purpose of the GERD, with an objective function as follows:

$$Max \quad E = \sum_{t=1}^{T} P_t \cdot \Delta t \;, \quad P_t = \eta \cdot g \cdot \rho \cdot Q_t^P \cdot H_t^P / 1000 \tag{1}$$

where E is the sum of hydroelectricity generation (kW h); P_t is the power generation output in period t (kW); T is the total number of operational periods and Δt is the time (h) of a single period (one month); η is the dimensionless hydropower generation efficiency of the turbines (set as 0.85 in this study); g is the gravitational acceleration (m/s²); ρ is the water density (kg/m³); and Q_t^P and H_t^P are the reservoir release (m³/s) and the average power head (m) in period t, respectively.

Physical and operational reservoir constraints are listed as below.

(a) Water balance:

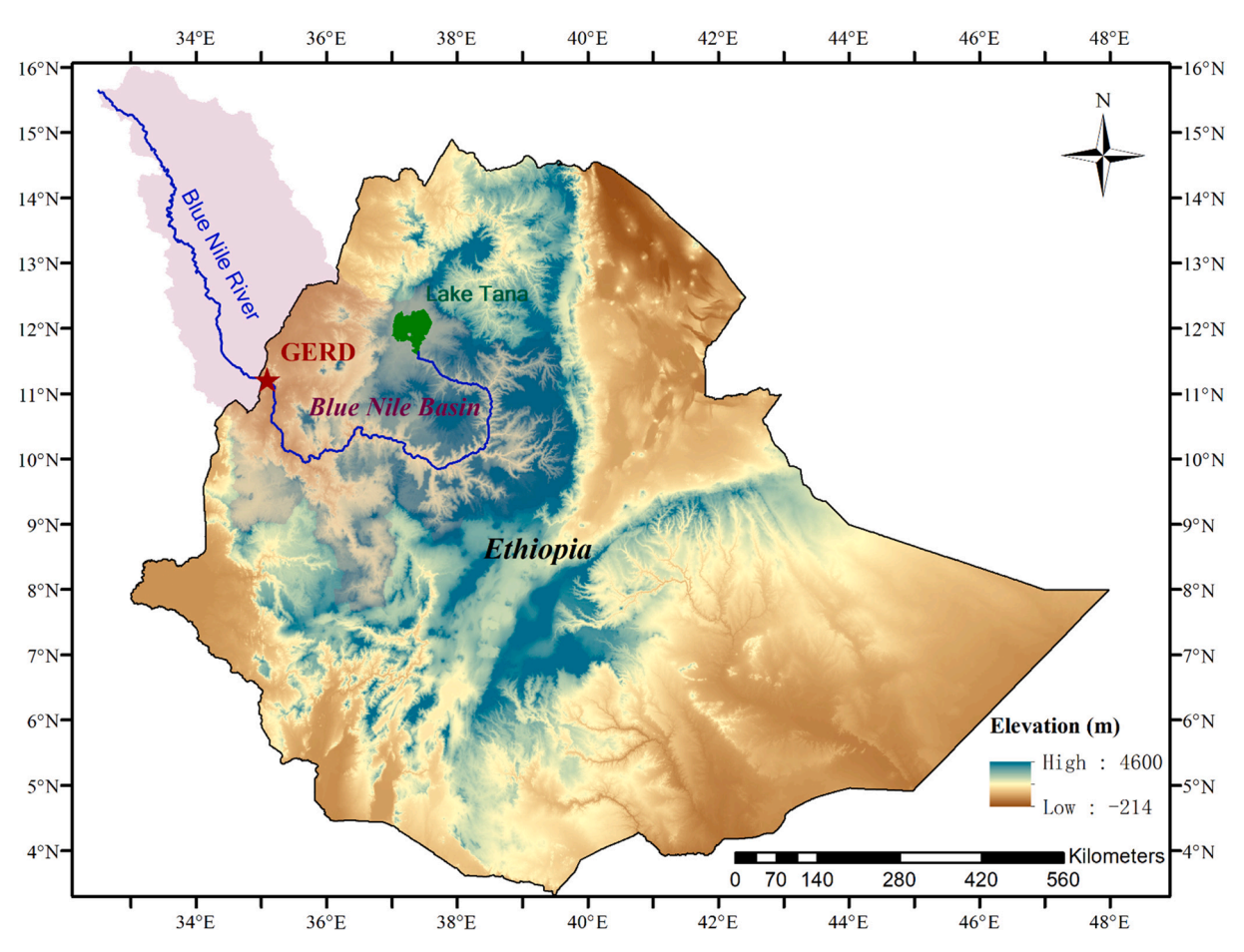


Fig. 1. The Blue Nile basin with Ethiopia country borders and the location of the GERD reservoir.

$$S_{t+1} = S_t + \left(Q_t^{in} - Q_t^{out}\right) \cdot \Delta t - EP_t \tag{2}$$

where S_t and S_{t+1} are reservoir storage (m³) in period t and t+1, respectively, Q_t^{in} represents reservoir inflow (m³/s) in period t, Q_t^{out} is reservoir release (m³/s) in period t, and EP_t is the sum of evaporation and seepage from the reservoir (m³) in period t.

(b) Reservoir capacity limits (Jameel, 2014):

The reservoir structural and operational constraints can be expressed as:

$$S^{min} \leq S_t \leq S^{max} \tag{3}$$

where S^{min} and S^{max} are the minimum and maximum allowable reservoir storage (m³), respectively.

Additionally, S^{begin} and S^{end} represent the initial and final reservoir storage (m³) for simulations, respectively, and are prescribed as:

$$S_t = \begin{cases} S^{begin} & t = 1 \\ S^{end} & t = T \end{cases}$$
 (4)

(c) Reservoir release limits:

The reservoir release constraints are expressed as:

$$QL_t \leqslant Q_t^{out} \leqslant QU_t \tag{5}$$

where QL_t and QU_t are the minimum and maximum release (m³/s) in period t, respectively. The expected guidelines for GERD reservoir water release are not explicitly available, thus releases are set lower than the maximum reservoir inflow during the high-flow season to avoid

downstream floods.

(d) Power generation limits (Tesfa, 2013):

$$PL_t \leqslant P_t \leqslant PU_t$$
 (6)

where PL_t and PU_t are the minimum and maximum power limits (kW) in period t, respectively.

3.2. Improved CEEMDAN method

Large-scale ocean-climate phenomena (e.g. the El Niño-Southern Oscillation, Pacific Decadal Oscillation, and Atlantic Multi-decadal Oscillation) modulate climate and hydrologic variables, namely precipitation and streamflow, at unique frequencies and timescales (Dettinger et al., 2000; McCabe et al., 2007; Nalley et al., 2016; Nowak et al., 2012). The influence of such phenomena at varying time-scale is apparent on Blue Nile streamflow (Eldaw et al., 2003; Taye and Willems, 2012; Zaroug et al., 2014), which can be decomposed into many nonlinear oscillatory patterns with different frequencies.

Numerous methods, including fast Fourier transform (Cochran et al., 1967), wavelet transform (Torrence and Compo, 1998), and empirical mode decomposition (EMD) (Huang et al., 1998; Huang and Wu, 2008; Wu and Huang, 2004), are available for streamflow decomposition. Of these three methods, only EMD is not subject to linear and stationary assumptions (Wu et al., 2007). The process for applying EMD method is as follows:

Step 1: Select all local maxima and minima and connect them with two cubic splines as the upper and lower envelops, respectively.

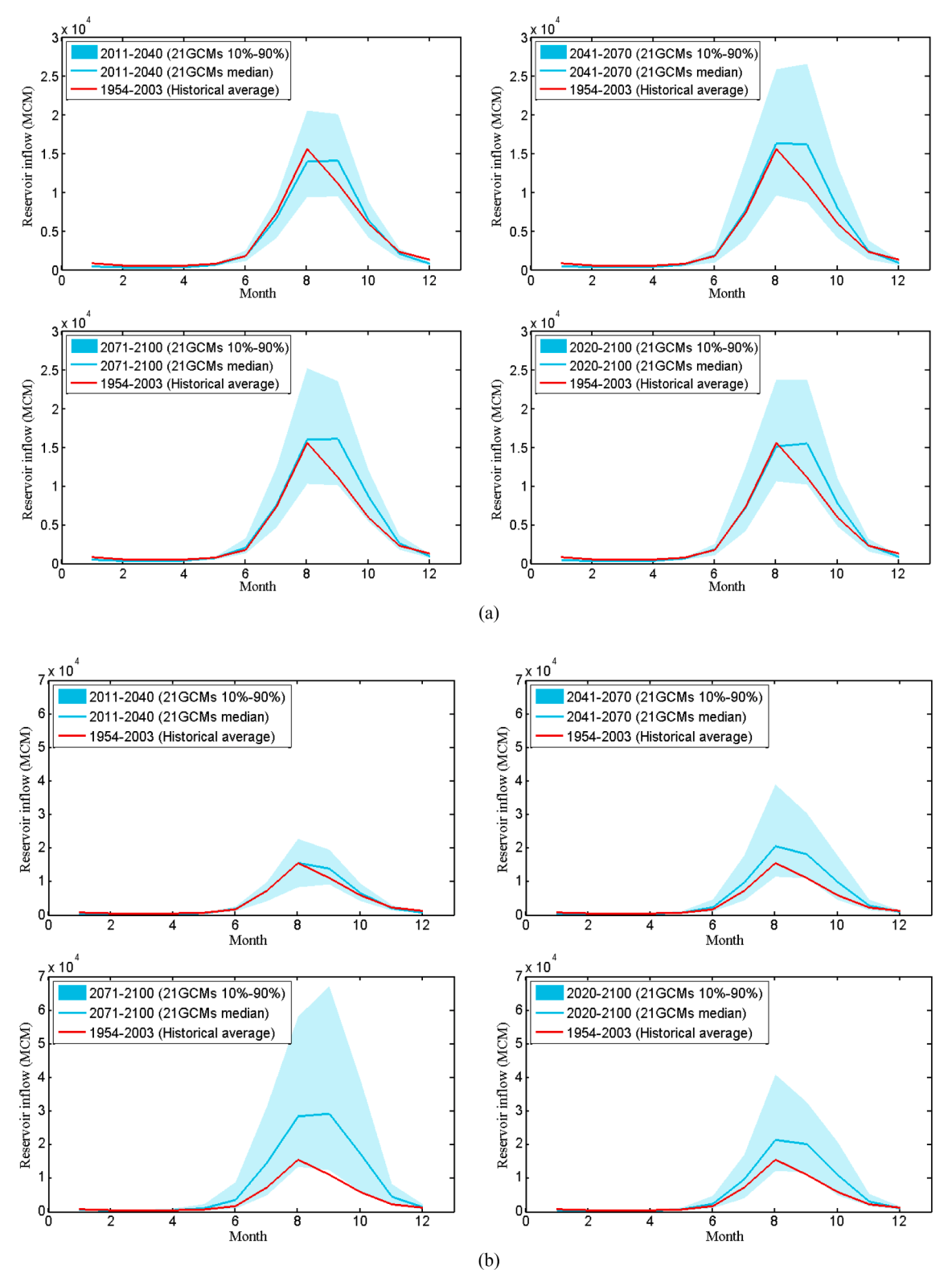


Fig. 2. Comparison of historical and future's GERD reservoir inflow for 21 GCMs in scenario (a) RCP4.5 and (b) RCP8.5.

Step 2: Define the average of the upper and the lower envelops as the intrinsic mode function (IMF), in which the difference between the number of maxima or minima and the zero-crossings must be equal to zero or one

Step 3: Obtain the residual by finding the difference between the original signal (streamflow series) I and the IMF.

Step 4: Repeat Steps 1–3 until the envelops are symmetric (with respect to a zero mean), at which point the streamflow signal is decomposed into several IMFs and one residual.

To overcome mode mixing issues and redundant IMFs, the EMD is modified into an ensemble empirical mode decomposition (EEMD) form (Wu and Huang, 2009). By adding white noise to the original signal, the

EEMD can avoid IMFs with widely disparate scales and preserve the physical uniqueness of the decomposition. However, the sum of the decomposed modes and the final trend from the EEMD will contain residual noise. To address this and obtain components with less noise, the improved Complete Ensemble Empirical Mode Decomposition with Adaptive Noise (CEEMDAN) as proposed by (Colominas et al., 2014) is applied here for GERD reservoir inflow decomposition. For more details about EMD, EEMD, and CEEMDAN, please refer to (Wu and Huang, 2004), (Wu and Huang, 2009), and (Colominas et al., 2014) respectively.

To isolate streamflow frequency information, the streamflow time-series is decomposed into unique frequency components using the improved CEEMDAN method (e.g. GCM3: BNU-ESM; Fig. 3), based on a 30-year streamflow series. The frequency of the intrinsic mode functions (IMF) decreases from sub-annual to long-term trend and are labeled as IMF 1 to IMF 8. IMF 1 and IMF 2 illustrate sub-seasonal changes while IMF 3 is annual, explaining inter-annual cycles. IMF 4–7 represent multi-year to decadal frequencies, and IMF 8 represents the trend of the streamflow across the 30-year period. IMF 8 is close to the inflow trend obtained from linear regression (Fig. 3(a)) and IMF 3 has a 12 month cycle, thus the improved CEEMDAN method may be able to accurately provide streamflow frequency information at least in terms of trend and 12 month cycles.

The decomposed IMFs are further divided into 4 categories: highfrequency (sub-annual), medium-frequency (annual), low-frequency (multi-year to decadal), and trend. To understand the impact of each frequency category, it is removed, and the streamflow series is reconstructed based on the remaining IMFs. This is denoted as frequencyremoved streamflow and reservoir operating rules extracted from this series as frequency-removed rules. Note that frequency-removed streamflow still corresponds to normal streamflow volume. Also, the IMF 8 here is not centered on zero, thus the mean is added back into the streamflow data after it is removed. The frequency-removed streamflow results for 2021-2050 (e.g. GCM3: BNU-ESM; Fig. 3(b)) show that the high, medium and low frequency categories explain much more of the variance in streamflow than the trend. By removing one frequency category, the frequency-removed streamflow will not be affected by the removed frequency, thus the performance difference between the frequencyremoved rules and the rules derived by streamflow data directly (frequency-complete rules) indicates the impact of the removed frequency on reservoir operation.

3.3. Reservoir operating rules

3.3.1. RBF-based reservoir operating rules

The radial basis function (RBF) approach which can ensure flexibility to the structure of the reservoir operating rules and capability to deal with a large number of input variables (Deisenroth et al., 2013), is adopted to determine water release decisions. For more applications of RBF models in reservoir operation see (Giuliani et al., 2015). With this approach, the reservoir water release decision is defined as:

$$Q_t^{out} = \sum_{u=1}^U \omega_u \varphi_u(X_t) \quad t = 1, ..., T \quad 0 \leq \omega_u \leq 1$$
(7)

$$\varphi_{u}(X_{t}) = exp\left[-\sum_{m=1}^{M} \frac{\left((X_{t})_{m} - c_{m,u}\right)^{2}}{b_{u}^{2}}\right] \quad c_{m,u} \in [-1,1], b_{u} \in (0,1]$$
(8)

where U is the number of RBFs, $\varphi_u(\cdot)$ represents the u^{th} RBF and ω_u is the weight of the RBF, M is the number of input variables X_t , and \mathbf{c}_u and b_u are the M-dimensional center and radius vectors of the u^{th} RBF, respectively. Reservoir storage, inflow, and seasonal information τ_t (where τ_t refers to the position of the current period t within a water year, e.g., it equals 1 when t is $1(12 \times 0 + 1)$, $13(12 \times 1 + 1)$, $25(12 \times 2 + 1)$..., considering that there are 12 periods within a water year) are

selected as input variables, i.e., $X_t = (S_t, Q_t^{in}, \tau_t)$. The number of RBFs is determined through a sensitivity analysis by increasing the RBFs until the power generation of optimal solutions do not change significantly; here, four RBFs are used. Thus M=3 (three input variables), U=4 (four RBFs) and 20 parameters in the RBFs-based reservoir operating rules.

Three types of reservoir operation strategy or rules are discussed here (Fig. 4.) The "historical-based rules" and "future-based rules" represent rules extracted from historical and future reservoir inflow by optimizing the parameters in Eqs. (7) and (8) with the inputs of historical and future streamflow, respectively. Both approaches produce static rules, derived only once during a specific period. The "future-based rules" approach is conditioned on perfect future foresight and therefore prescribes operations leading to optimal power generation in the future; clearly this represents an upper (unrealistic) bound on performance of the RBFbased rules. As a compromise, we derive "adaptive operating rules" based on streamflow data proximal to when decisions are made. For example, reservoir operating rules extracted from 30-years of streamflow (e.g. 2020-2049) are used for the period 2050-2054. The periods 2020-2049 and 2050-2054 in the example are denoted as the extraction and application periods, respectively. We recalibrate and validate the rules every $5 \sim 10$ years and find that updating the rules at 5-year increments performs best and thus this strategy is used for all adaptive rules in this study. The comparison of historical-based, adaptive, and future-based rules in monthly power generation can be found in Appendix S1 (Fig. S1).

3.3.2. BMA-based reservoir operating rules

Bayesian model averaging (BMA) is a statistical approach to infer a probabilistic scheme by combining multiple possible competing models and has been implemented in reservoir operating rules derivations (Zhang et al., 2015). Suppose there exists K adaptive reservoir operating rules $(R_1, R_2, ..., R_K)$ from which K different reservoir release strategies are available at each time period. By using the improved CEEMDAN method, streamflow data can be decomposed into many IMFs with varying frequency and classified into several categories (e.g. high, medium and low frequency, and trend). In this study, K is equal to five: R_1 refers to frequency-complete rules derived by streamflow data directly, and R_2 , R_3 , R_4 , and R_5 refer to frequency-removed rules derived by excluding high, medium and low frequency, and trend information, respectively. More specifically for R2, R3, R4, and R5, the associated category of IMFs (e.g. high frequency for R2) is removed from the original streamflow data and the remaining IMFs are summed together to form a streamflow series without the corresponding (e.g. high frequency) information. As described in Eqs. (7) and (8), the rules R_1 , R_2 , R_3 , R_4 , and R_5 share the same structure (and same number of parameters). However, their parameters are optimized based on different types of streamflow time series (e.g., complete streamflow and streamflow without high frequency information). In this study, we optimize the parameters of rules R₁, R₂, R₃, R₄, and R₅ individually, by using the Dynamically Dimensioned Search (DDS) evolutionary algorithm (Tolson and Shoemaker, 2007).

According to the law of total probability, the reservoir release probability density function is expressed as follows:

$$p(Q_{out}|Q_{in}) = \sum_{k=1}^{K} p(Q_{out}|R_k, Q_{in}) p(R_k|Q_{in})$$
(9)

where $p(Q_{out}|R_k,Q_{in})$ is the release probability density function based on rule R_k and streamflow series Q_{in} . Given the adaptive rule R_k , Q_{out} is the deterministic function of Q_{in} (i.e., $Q_{out} = f_{R_k}(Q_{in})$), thus the $p(Q_{out}|R_k,Q_{in})$ equals one for $Q_{out} = f_{R_k}(Q_{in})$, otherwise it equals zero. $p(R_k|Q_{in})$ is the posterior probability of rule R_k given the streamflow series Q_{in} , which describes the probability that R_k is suitable to the reservoir operation with Q_{in} . The $p(R_k|Q_{in})$ is an unknown variable and must be estimated from the performance of adaptive rule R_k (the better R_k performs with Q_{in} , the higher the $p(R_k|Q_{in})$). The sum of the posterior model

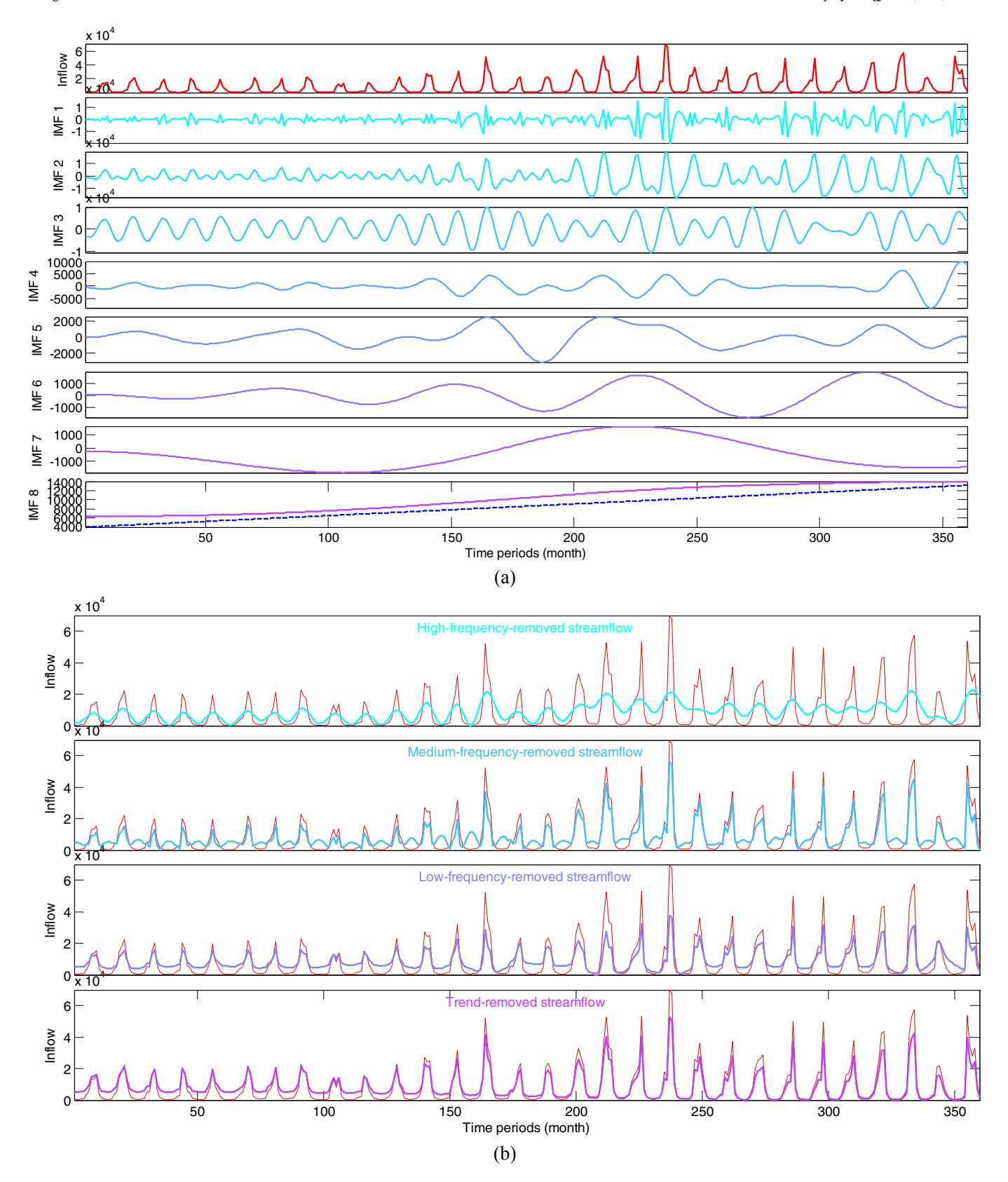
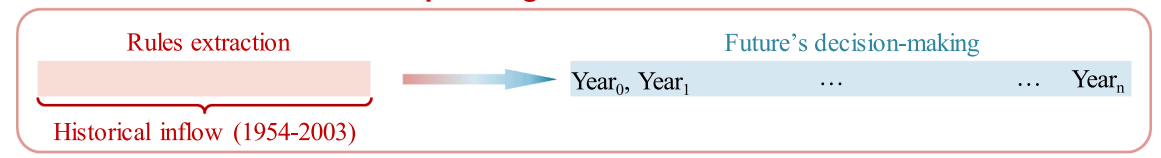
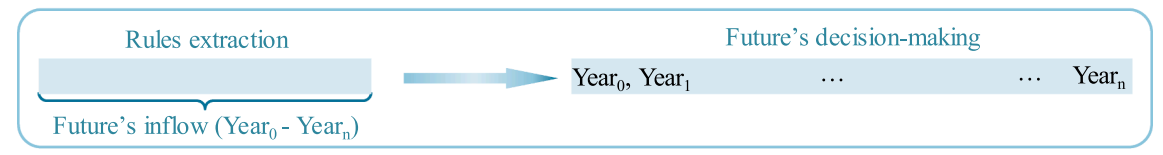


Fig. 3. Decomposition results of GERD monthly inflow and frequency-removed streamflow series during 2021–2050 for GCM 3: BNU-ESM in scenario RCP4.5. (a) Decomposition results of GERD monthly inflow, in which dash line refers to the streamflow trend extracted from linear regression; (b) Frequency-removed streamflow series, in which red line refers to original streamflow. (For interpretation of the references to colour in this figure legend, the reader is referred to the web version of this article.)

Historical-based reservoir operating rules



Future-based reservoir operating rules



Adaptive reservoir operating rules

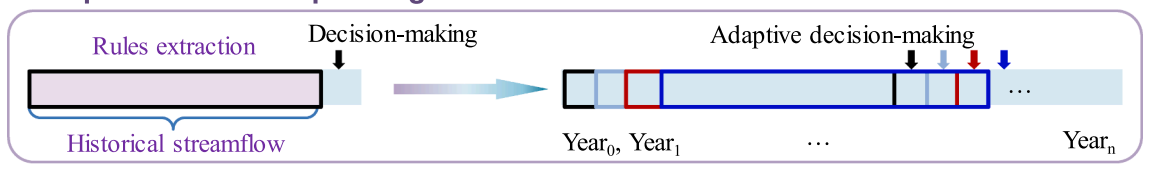


Fig. 4. Schematic illustration of different types of reservoir operating rules.

probabilities is equal to one (i.e., $\sum_{k=1}^K p(R_k|Q_{in})=1$), and the $p(R_k|Q_{in})$ can be regarded as a weight w_k . The reservoir release is then the posterior mean of the BMA model values:

$$Q_{out}^* = E[Q_{out}|Q_{in}] = \sum_{k=1}^K f_{R_k}(Q_{in})w_k$$
 (10)

where $f_{R_k}(Q_{in})$ refers to the water release obtained from rule R_k .

By comparing the reservoir operation performance of rules R_k (k=2,3,4,5) with R_1 during the application period, the impact of the frequency (high, medium and low) and trend information can be evaluated. The value of the frequency information F_k on reservoir operations during the period $T_1 \sim T_2$ ($\Delta T = T_2 - T_1$) in this study is defined as:

$$Value(F_k, \Delta T) = \sum_{t=T_1}^{T_2} [P(Q_t^{in}, R_1) - P(Q_t^{in}, R_k)] \qquad k = 2, 3, ..., K$$
 (11)

where P() is the function to calculate power generation. Given a reservoir state, both the average power head H_t^P and reservoir release Q_t^P in Eq. (1) can be calculated from reservoir inflow Q_t^{in} and rules R_k to get the power generation $P(Q_t^{in}, R_k)$.

In most cases, frequency-complete rules R_1 can capture the main features of frequency information in future streamflow and the $Value(F_k, \Delta T)$ is generally positive. However, if the k^{th} frequency signal is strong and changes significantly from the extraction to the application periods, then the rules derived from the extraction period with that k^{th} frequency signal will perform poorly in the application period. For the rules extraction with that signal removed, it will do better in the application period and the $Value(F_k, \Delta T)$ can be negative. In this case, the R_1 will be misleading and the weight applied to the rules extracted without the categorical frequency information should be increased.

To detect and mitigate the non-stationarity associated with different frequency information, the BMA model is extended to a dynamic model by updating the weight w_k based on the value of frequency information through Eqs. (12) and (13). Because R_k is obtained from the streamflow during the extraction period Q_{in}^k , the more similar streamflow during application period Q_{in} is to Q_{in}^k , the higher the w_k . Thus w_k here also reflects the degree of non-stationarity in streamflow between Q_{in}^k and Q_{in} .

$$z_k^{(j)} = \frac{Rank(Value(F_k, j-1)|Values) - 1}{0.5(K-1) \cdot K} + w_k^{(j-1)} \quad k = 1, 2, ..., K$$
 (12)

$$w_k^{(j)} = \frac{z_k^{(j)}}{\sum_{k=1}^K z_k^{(j)}}$$
 (13)

where $w_k^{(j)}$ is the weight applied to releases at stage j, $Rank(Value(F_k, j-1)|Values)$ is the descending rank of the frequency information value $Value(F_k, j-1)$ among all ensemble members (K members in total). More specifically, the $Rank(Value(F_k, j-1)|Values)$ will be 1 (K) for the greatest (least) information value as defined in Eq. (11).

In this study, the weight is updated annually according to the performance of BMA-based rules. Considering that the weights are updated much more frequently than the parameters of reservoir operating rules, BMA model parameters and RBF-based rule parameters are not optimized simultaneously. Initially, the weight of R_1 is equal to one, (i.e., frequency-complete rules are fully trusted, $w_1^{(0)}$ is set to one while $w_k^{(0)}(k=2,3,...,K)$ is set to zero). Then $w_k^{(j)}$ is updated according to $Value(F_k,X)$; a lower $Value(F_k,X)$ will lead to a higher weight on the rules extracted without the frequency information F_k . In this way, the $p(R_k|Q_{in})$ in Eq. (9) can be estimated from the performance of reservoir operating rules R_k (k=1,2,3,4,5). Because the frequency-complete rules R_1 are effective in most cases, additional weight w_a is added for each update of $z_1^{(j)}$ in the Eq. (12) as:

$$z_1^{(j)} = \frac{Rank(Value(F_1, j-1)|Values) - 1}{0.5(K-1) \cdot K} + w_1^{(j-1)} + w_a$$
 (14)

where w_a ranges from 0 to 1 and is determined from the validation of the BMA-based rules at stage j-1 for maximum power generation. More specifically, increasing w_a from 0 to 1 (e.g., 0, 0.1, 0.2,...,1) and validating the performance of BMA-based rules at stage j-1, the w_a values that produce the greatest power generation are selected for the stage j (Fig. 5).

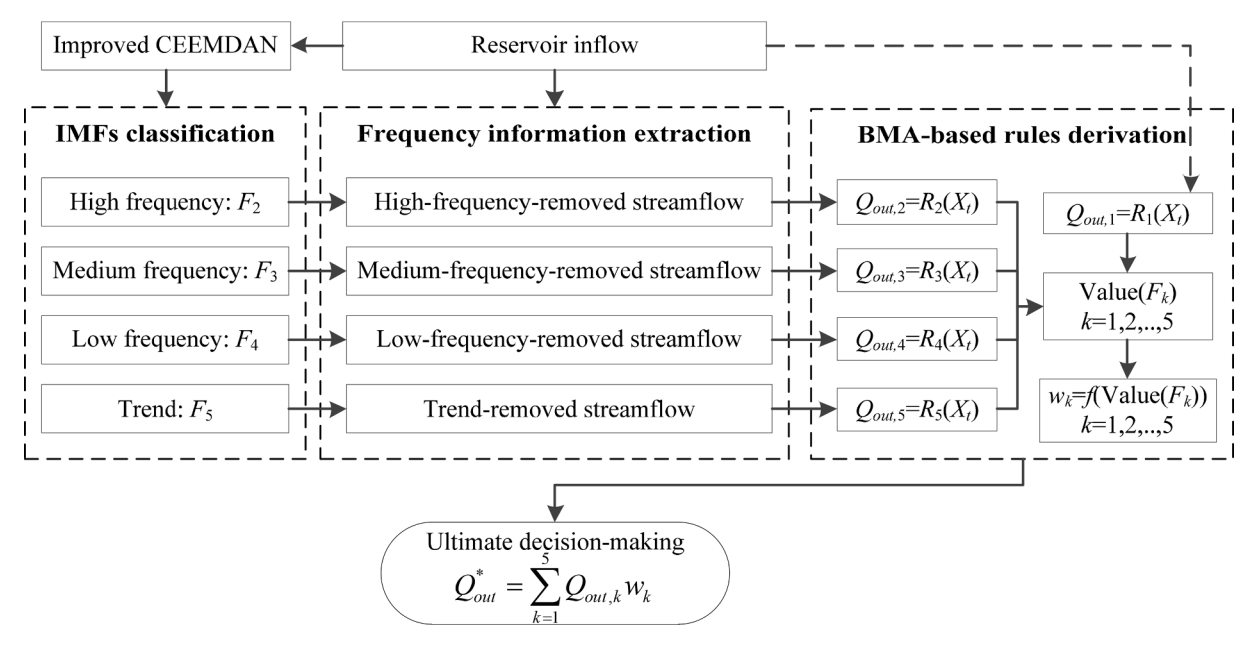


Fig. 5. Procedure of the BMA-based reservoir operating rules derivation.

4. Results and discussion

4.1. Impacts of streamflow frequency information on adaptive reservoir operations

To evaluate the impact of streamflow frequency information on adaptive reservoir operations, the frequency-removed rules are applied across 2020-2100 for each category and GCM, independently, and compared against frequency-complete rules (Fig. 6.) The power generation output brought from all types of frequency information (which is calculated by subtracting the output of frequency-removed rules with the output of frequency-complete rules) is predominantly greater than zero, implying that including all types of frequency information has a beneficial impact on power generation on average (Fig. 6.). Additionally, the output of frequency-removed rules (Pwof) is occasionally greater than the output of frequency-complete rules (Pnorm). More specifically, Pwof > Pnorm occurs for 32%, 43%, 38%, and 48% (25%, 36%, 35%, and 44%) of operational periods (years) for high, medium, low frequency and trend -removed rules, respectively, under scenario RCP4.5 (RCP8.5) (see bottom Fig. 6). Thus trend information leads to the highest percentage of periods with P_{wof} > P_{norm}, which indicates that the trend information is more likely to be non-stationary than other frequency categories.

The average of frequency information value ($Value(F_k, \Delta T)$ in Eq. (11), the difference between power generation of frequency-removed rules and frequency complete rules) across all GCMs (lines in Fig. 7) and the rank of frequency information value (bars in Fig. 7) indicate that high frequency information typically contributes the most to power output whereas the trend provides the least (i.e., the sub-seasonal variability (short-term variability) in streamflow has greater impact than the trend (long-term variability) on reservoir operation, which is consistent with the findings from Herman and Giuliani (2018)); the medium and low frequency information, although contributing less than the high frequency, are still appreciable. More specifically, highfrequency-removed rules produce approximately 120 MW, 200 MW, and 180 MW power output more than frequency-complete rules during the periods 2011-2040, 2041-2070, and 2071-2100, respectively for RCP4.5, (140 MW, 240 MW, and 290 MW, respectively, for RCP8.5). Except for 2071-2100 under scenario RCP8.5, low frequency information contributes more to power output than the medium frequency information on average. For example, medium frequency contributes 157

MW and 124 MW (surpassing 130 MW and 100 MW from low frequency information) annually during 2020 \sim 2100 for GCM3 and GCM15, respectively, under scenario RCP4.5. The reason is that the medium frequency information has been partially included in the RBF-based rules (in Eqs. (7) and (8)) in which the input variable τ_t (the position of the current period t within a water year) shares the same (annual) cycle as the medium frequency.

The lack of frequency information clearly affects how the adaptive reservoir operating rules are constructed. When a certain frequency is removed from the streamflow series during rules extraction, the derived reservoir operating rules will fail to appropriately adapt to future streamflow when this feature (frequency) is influential for reservoir decision-making. However, if the frequency-removed rules perform better than the frequency-complete rules ($P_{wof} > P_{norm}$) in the application period (Table 2), it can be inferred that non-stationarity exists (streamflow in the rules extraction period is not consistent with that in the rules application period) for the removed frequency. It is worth noting that not all situations with Pwof > Pnorm in Table 2 indicate streamflow non-stationarity; instead, Pwof > Pnorm during some times could be caused by noise, especially when Pwof and Pnorm are close to each other (e.g., the median frequency for GCM21 under scenario RCP4.5 during 2071–2100, Table 2). But the more frequently P_{wof} > P_{norm} occurs, the more likely streamflow non-stationarity exists. It can be inferred that streamflow non-stationarity is significant when considering the trend category, specifically for 12 GCMs during 2011 \sim 2040 under scenario RCP4.5 (Table 2.) Removing streamflow information at appropriate frequencies (e.g. when $P_{wof} > P_{norm}$) could possibly improve adaptive reservoir operations.

4.2. BMA-based adaptive reservoir operating rules

4.2.1. Non-stationarity and adaptive reservoir operating rules

Given the apparent non-stationarity in streamflow, specified by period, GCM, and frequency category (Table 2), future reservoir operations will likely benefit if the non-stationarity is detected and considered in the rules extraction stage. Detection, however, is challenging, given that future streamflow is unknown and the non-stationarity characteristics may change throughout the reservoir operation period. Thus, it is assumed that the probability of non-stationarity occurrence in the future is related with that in the past. More specifically, if streamflow non-stationarity at one frequency is detected in the past, it can be

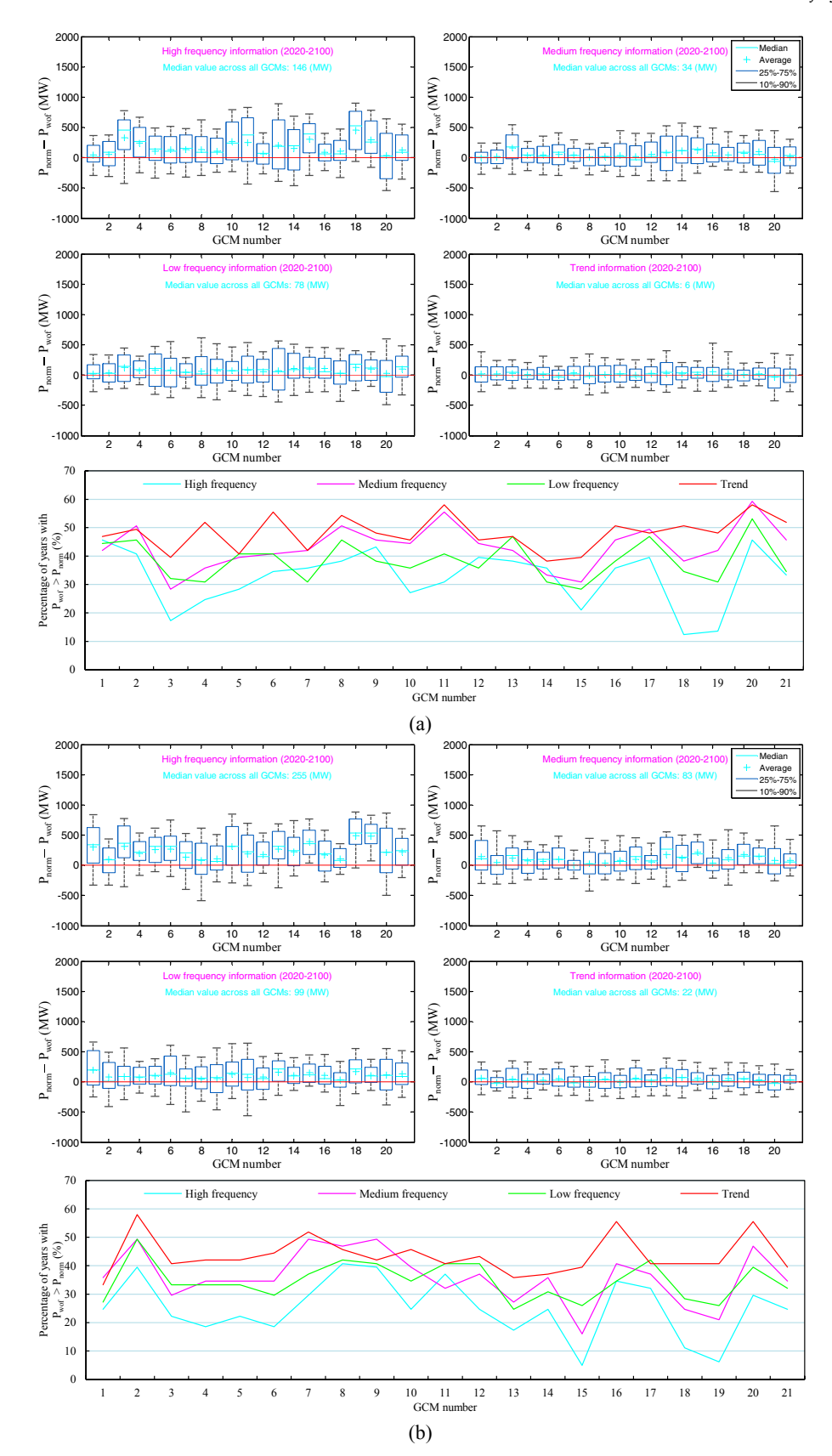


Fig. 6. Difference in power generation output between frequency-removed rules and frequency-complete rules for 21 GCMs in scenario (a) RCP4.5 and (b) RCP8.5. " P_{wof} " and " P_{norm} " refer to the power output of frequency-removed rules and frequency-complete rules, respectively.

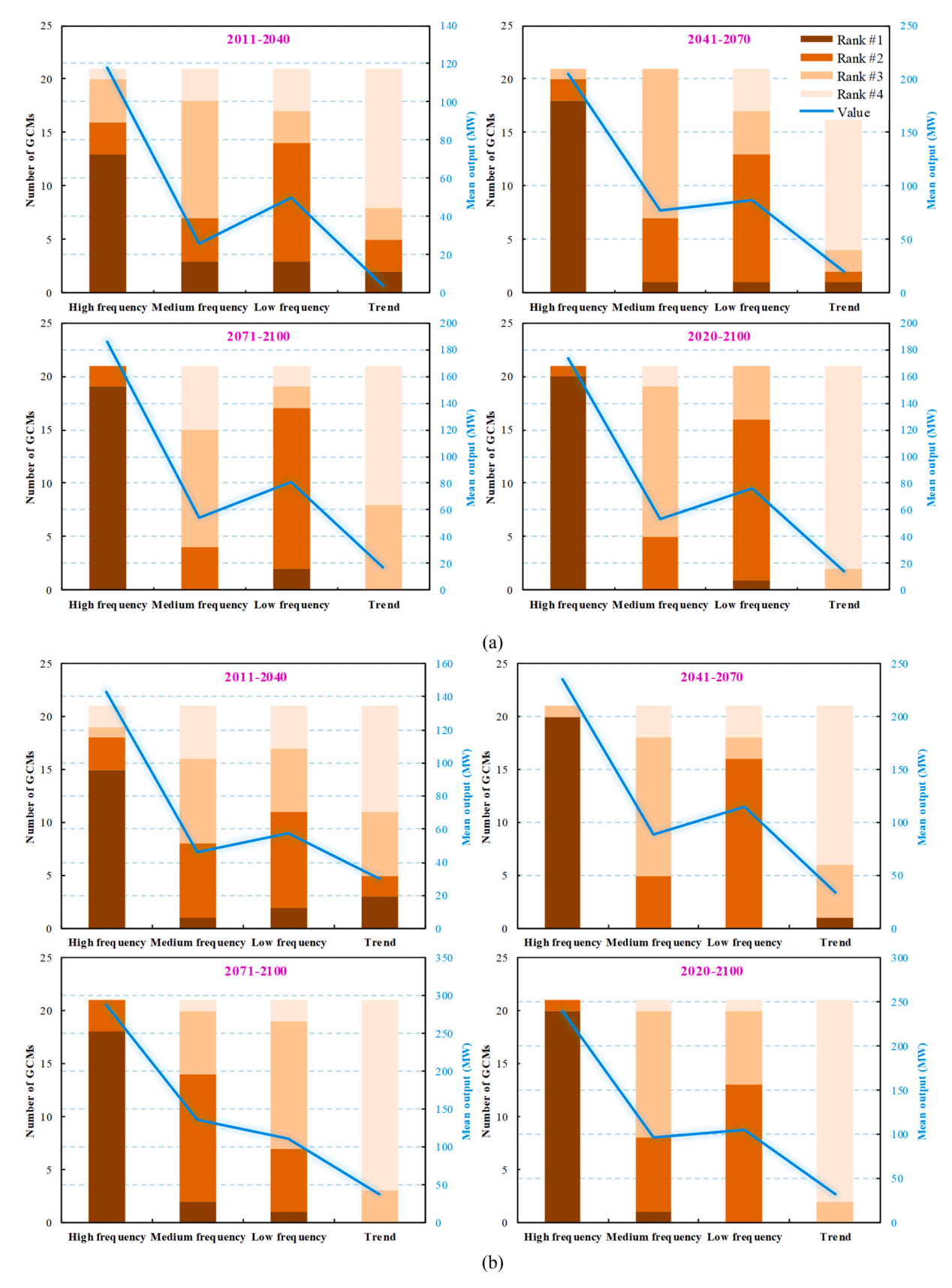


Fig. 7. Rank and power output of high, medium and low frequency, and trend information for 21 GCMs in scenario (a) RCP4.5 and (b) RCP8.5. Line and bar charts represent the rank and output, respectively, the darker bar means more important frequency and the length of the bars means the number of GCMs in which a certain frequency information ranks the first, second, third or fourth place in adaptive reservoir operation.

Table 2 Monthly mean power output (MW) based on $P_{norm} - P_{wof}$; in parentheses, percent of years $P_{wof} > P_{norm}$ for different periods under RCP4.5 and RCP 8.5.

Scenarios	Time periods	GCMs	High frequency	Medium frequency	Low frequency	Trend
RCP4.5	2011–2040	GCM1	-91(53%)	-84(53%)	-102(63%)	-47(57%
		GCM2	-27(50%)	47(33%)	-46(63%)	14(40%)
		GCM3	340(13%)	9(43%)	68(47%)	-19(57%
		GCM4	263(20%)	25(37%)	140(20%)	-15(47%
		GCM7	101(40%)	2(50%)	20(37%)	-8(30%)
		GCM9	122(40%)	19(43%)	61(37%)	-6(53%)
		GCM10	-11(53%)	-29(60%)	-42(47%)	15(43%)
		GCM11	402(10%)	47(57%)	121(33%)	-10(63%
		GCM13	-40(53%)	-29(60%)	-46(57%)	-36(60%
		GCM15	101(33%)	47(37%)	70(30%)	-22(40%
		GCM16	84(50%)	34(60%)	23(53%)	-11(57%
		GCM19	148(33%)	22(47%)	8(40%)	-24(50%
		GCM20	31(43%)	14(50%)	32(43%)	-10(53%
		GCM21	60(43%)	-2(53%)	42(43%)	-4(50%)
	2041-2070	GCM8	150(30%)	32(47%)	47(47%)	-17(60%
		GCM9	42(53%)	6(50%)	-10(47%)	-5(50%)
		GCM11	221(37%)	53(47%)	102(43%)	-2(57%)
		GCM12	20(53%)	72(37%)	-18(43%)	58(33%)
		GCM17	85(37%)	26(50%)	-28(53%)	18(47%)
		GCM20	74(50%)	-53(70%)	-11(60%)	-69(70%
	2071-2100	GCM2	68(40%)	-10(57%)	48(43%)	4(60%)
		GCM4	168(37%)	27(40%)	58(33%)	-2(50%)
		GCM6	182(27%)	30(50%)	38(40%)	-25(57%
		GCM8	97(53%)	-7(53%)	123(43%)	44(50%)
		GCM11	189(40%)	20(57%)	93(40%)	-10(57%
		GCM14	29(43%)	-36(50%)	-10(40%)	-15(50%
		GCM20	11(47%)	-36(57%)	57(53%)	-27(53%
		GCM21	158(30%)	-5(43%)	96(40%)	13(47%)
RCP8.5	2011-2040	GCM1	-99(57%)	-6(47%)	-4(40%)	-66(53%
		GCM4	257(20%)	79(37%)	78(37%)	-25(33%
		GCM5	62(37%)	28(43%)	24(50%)	-40(50%
		GCM8	-70(53%)	-8(53%)	60(40%)	20(50%)
		GCM10	195(37%)	-39(53%)	-4(37%)	-49(50%
		GCM13	114(33%)	70(40%)	82(37%)	-40(63%
		GCM14	150(47%)	36(57%)	75(40%)	-15(47%
	2041-2070	GCM7	26(40%)	9(60%)	-13(47%)	-38(60%
		GCM8	148(33%)	-21(53%)	20(47%)	-32(47%
		GCM10	251(27%)	84(37%)	201(27%)	-36(60%
		GCM16	141(40%)	-10(47%)	43(37%)	-8(53%)
		GCM17	53(47%)	76(50%)	-32(57%)	91(43%)
		GCM20	208(30%)	51(57%)	139(40%)	-10(53%
	2071-2100	GCM2	83(33%)	76(50%)	-7(63%)	-35(63%
		GCM4	144(20%)	107(30%)	65(30%)	-1(43%)
		GCM8	74(43%)	44(43%)	2(40%)	-20(47%
		GCM12	236(23%)	61(40%)	40(50%)	-16(53%

assumed to exist similarly in the future.

After detection of possible streamflow non-stationarity (Eq. (11)), water release decision weights for the different rules are updated (Eqs. (12) and (13); (Fig. 8)). The weight of frequency-complete rules fluctuates with the time, but it is always greater than the weight of frequency-removed rules. Also, trend-removed rules receive the largest weight for most GCMs in comparison to other frequency-removed rules, indicating that streamflow non-stationarity is likely most significant for the trend category (consistent with the findings in Fig. 6 and Table 2). By updating the weight $w_k^{(j)}$ and merging the water releases obtained from different types of rules through Eq. (10), the BMA-based rules incorporate non-stationarity from different frequency categories into reservoir decision making in a dynamic way.

The cumulative mean power output from the BMA-based rules is compared with normal rules (frequency-complete rules) (Fig. 8.) Except for GCM3, 12, 16, and 19 under scenario RCP4.5 and GCM3, 9, 12, 15, 18, and 21 under scenario RCP8.5, the BMA-based outcomes are equal to or superior to outcomes utilizing normal rules. More specifically, the increase in power output through 2100 from the BMA-based rules is greater than 10,000 MW·month (7.3 GW·h) for GCM1, 2, 8, 10, 11, 13, and 20 under RCP4.5, and greater than 20,000 MW·month (14.6 GW·h) for GCM8 and GCM10 under RCP8.5. This increase in power generation cannot necessarily be generalized, as different frequency-removed

categories contribute uniquely by GCM, which can be inferred from the weights of different types of reservoir operating rules in Fig. 8. For example, the increase in cumulative output during $2020\sim2030$ for GCM2 under RCP4.5 is mainly supplied by the high frequency-removed and low frequency-removed rules, whereas increases during $2040\sim2050$ for GCM8 under RCP4.5 is attributable to the trend-removed and medium frequency-removed rules, respectively (Fig. 8(a).) In some cases (e.g., GCM 15 under RCP8.5), BMA-based rules produce less overall power than normal rules (Fig. 8(b)), implying that non-stationarity is minimally evident throughout the period (the weight of normal adaptive rules has its highest value and does not change during $2025\sim2100$), and BMA-based rules could be inferior to normal rule.

The performance of BMA-based rules is further investigated by analyzing changes in monthly mean output (Fig. 9.) Generally, power generation based on the high frequency-removed rules illustrates the largest (negative) difference with normal adaptive rules; trend-removed rules illustrate the least (closest to zero.) Since normal adaptive rules have their parameters updated every 5 years in this case study, the streamflow trend becomes mostly insignificant and thus has no measurable impact on power generation. Although the BMA-based rules predominantly perform better than or similar to normal rules in cumulative or mean output, the improvement is limited (and BMA-based rules may be even inferior to normal rules in some cases). The reason is that

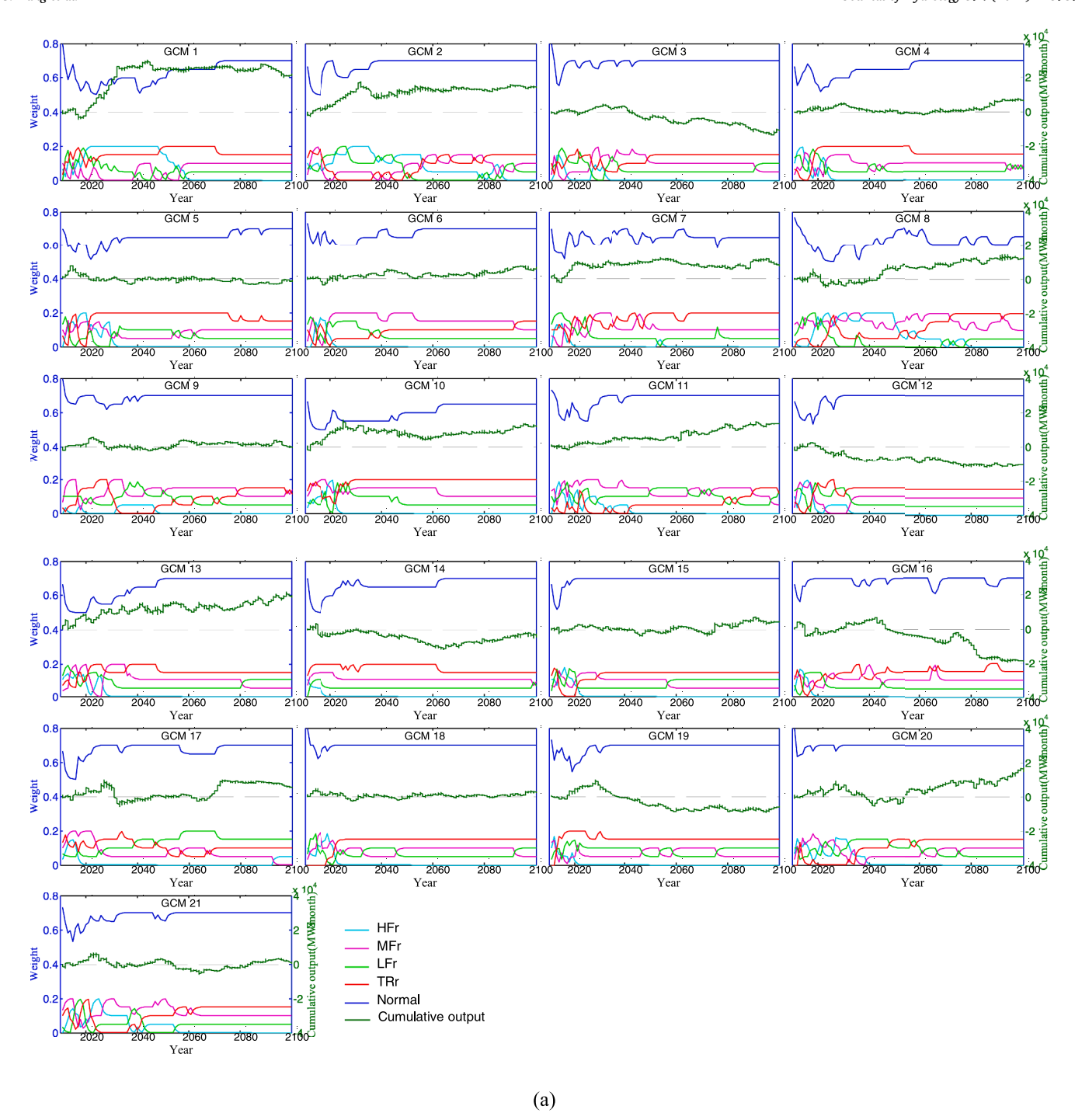


Fig. 8. Weight of different types of reservoir operating rules and cumulative output of BMA-based rules compared with normal adaptive rules for 21 GCMs in scenario (a) RCP4.5 and (b) RCP8.5. "HFr", "MFr", "LFr", and "Normal" denote the weight of high-frequency-removed, medium-frequency-removed, low-frequency-removed, trend-removed, and frequency-complete rules, respectively.

normal adaptive rules have partially considered possible nonstationarity (especially based on trend information) by recalibrating the parameters every 5 years.

4.2.2. Performance of BMA-based rules in firm output

In addition to considering maximum power generation, the BMA-based rules are also evaluated for their ability to improve firm power generation for various reliability levels (Fig. 10.) Reliability is conditioned on each GCM time-series individually; a 95% reliability implies that a power output threshold is met or exceeded in 95% of the months during the given period for that GCM. In general, BMA-based rules

improve firm output across most GCMs and reliability levels, with the largest increase in firm output (for reliability of 95%) during 2011 \sim 2100 (greater than350 MW [105%] per month for RCP4.5 and 450 MW [180%] per month for RCP8.5; Fig. 10). Considering RCP8.5 only, the BMA-based model is superior in nearly all cases. Thus the BMA-based rules obtain an advantage over normal adaptive rules mainly in terms of firm output (instead of total or mean output).

As shown in Fig. 9(b), BMA-based rules could perform worse than normal rules in terms of mean output during $2011 \sim 2020$ for some GCMs (such as GCM18 in scenario RCP8.5). The comparison between the BMA-based and normal rules in density distribution and boxplot of

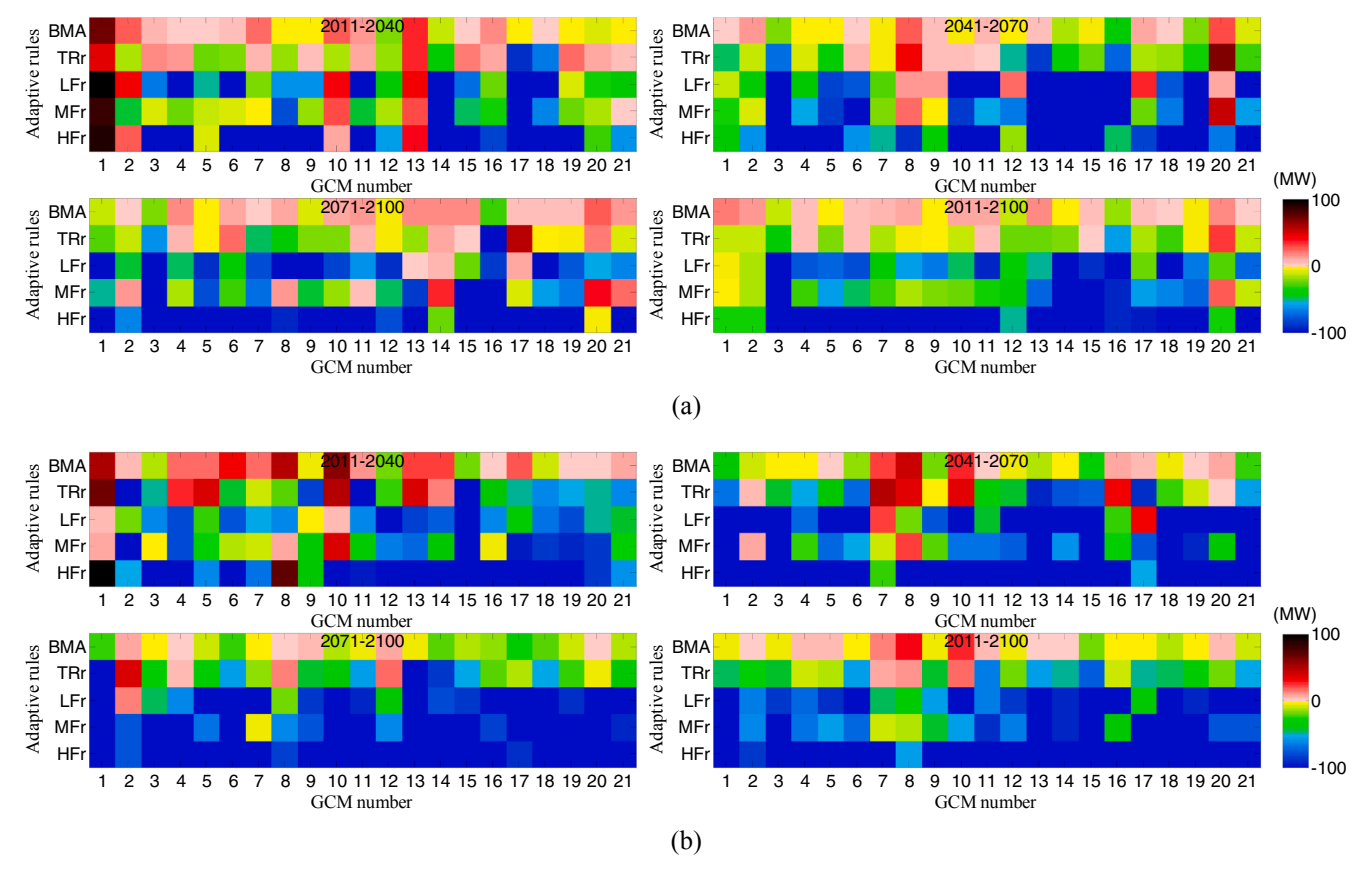


Fig. 9. Monthly mean output increased by using information-removed and BMA-based reservoir operating rules for 21 GCMs in scenario (a) RCP4.5 and (b) RCP8.5. "HFr", "MFr", "LFr", and "TRr" denote the reservoir operating rules extracted with high-frequency removed, medium-frequency removed, low-frequency removed, and trend removed streamflow, respectively; "BMA" denotes the BMA-based adaptive reservoir operating rules.

monthly output during 2011 \sim 2020 under GCM18 in scenario RCP8.5 (Fig. 11(b) and (d)) (BMA-based model results in lower mean output than the model conditioned on normal rules) illustrates that BMA-based rules tend to increase low-level (<3000 MW) outputs and the increment mainly occurs in June, July, and August. Comparing the case when the BMA-based model results in higher mean output than the model using normal rules (Fig. 11(a) and (c)) also illustrates the advantage of BMA-based rules in obtaining greater power generation when the output is lower than 2000 MW. This occurs because the BMA-based rules can avoid extremely high or low releases (in mistake) by averaging releases from normal (frequency-complete) and frequency-removed rules. Thus the BMA-based rules can avoid extremely low output and obtain more consistent outputs than normal rules (see the density distribution of monthly output in Fig. 11(a)).

Averaging across all GCMs, the BMA-based rules produce more firm power output than normal adaptive reservoir operating rules for all levels of reliability (from 80% to 100%) (Table 3.) For example, the percentage increase in firm power output of BMA-based rules during 2011 ~ 2100 ranges from 3.9% to 69.1% and 5.4% to 129.4% for RCP4.5 and RCP8.5, respectively. Additionally, the percentage increase in firm output increases as the reliability increases, to over 35% and 50% during all time periods for RCP4.5 and RCP8.5, respectively, when the reliability is close to 100%. This advantage in firm output is particularly significant when considering demand for high power generation reliability, which can be crucial in the manufacturing sector (Allcott et al., 2016), and may lead to economic benefits now and into the future.

5. Conclusions

Adaptive reservoir operating rules generally outperform static or historical-based rules in water resources management under nonstationary conditions. However, conventional adaptive rules do not consider potential non-stationarity at multiple time scales, which is rarely investigated. This study illustrates a strategy to incorporate streamflow non-stationarity information for different time scales simultaneously into adaptive reservoir operating rules and potential value over conventional (normal) adaptive rules.

To detect the streamflow non-stationarity at different time scales, streamflow time series are decomposed into different frequency categories and their impacts on reservoir operation is evaluated. Subsequently, the non-stationarity information of different frequency categories is incorporated into adaptive reservoir operating rules using a BMA method. The performance of the Bayesian adaptive reservoir operation framework is evaluated for the GERD reservoir operation in Ethiopia using monthly streamflow simulated from 21 GCMs under scenarios RCP4.5 and RCP8.5. High, medium, low, and trend information extracted from the streamflow time series is shown to affect GERD reservoir operations diversely. Recognizing streamflow non-stationarity at different frequencies and removing it from the original streamflow time series can improve adaptive reservoir operations.

Overall, high frequency (sub-seasonal) information has the greatest impact on power generation, while the most significant non-stationarity in streamflow is associated with the trend information for adaptive GERD reservoir operation. Additionally, the Bayesian adaptive framework can recognize streamflow non-stationarity at different frequency categories and mitigate its impacts on normal adaptive reservoir operating rules. Thus, the Bayesian adaptive rules predominantly outperform normal adaptive rules considering power generation, especially in terms of firm power output. In general, firm output increases under the Bayesian framework as the power generation reliability increases; this implies that the Bayesian adaptive rules are preferable when high power generation reliability is required. Although the Bayesian adaptive rules

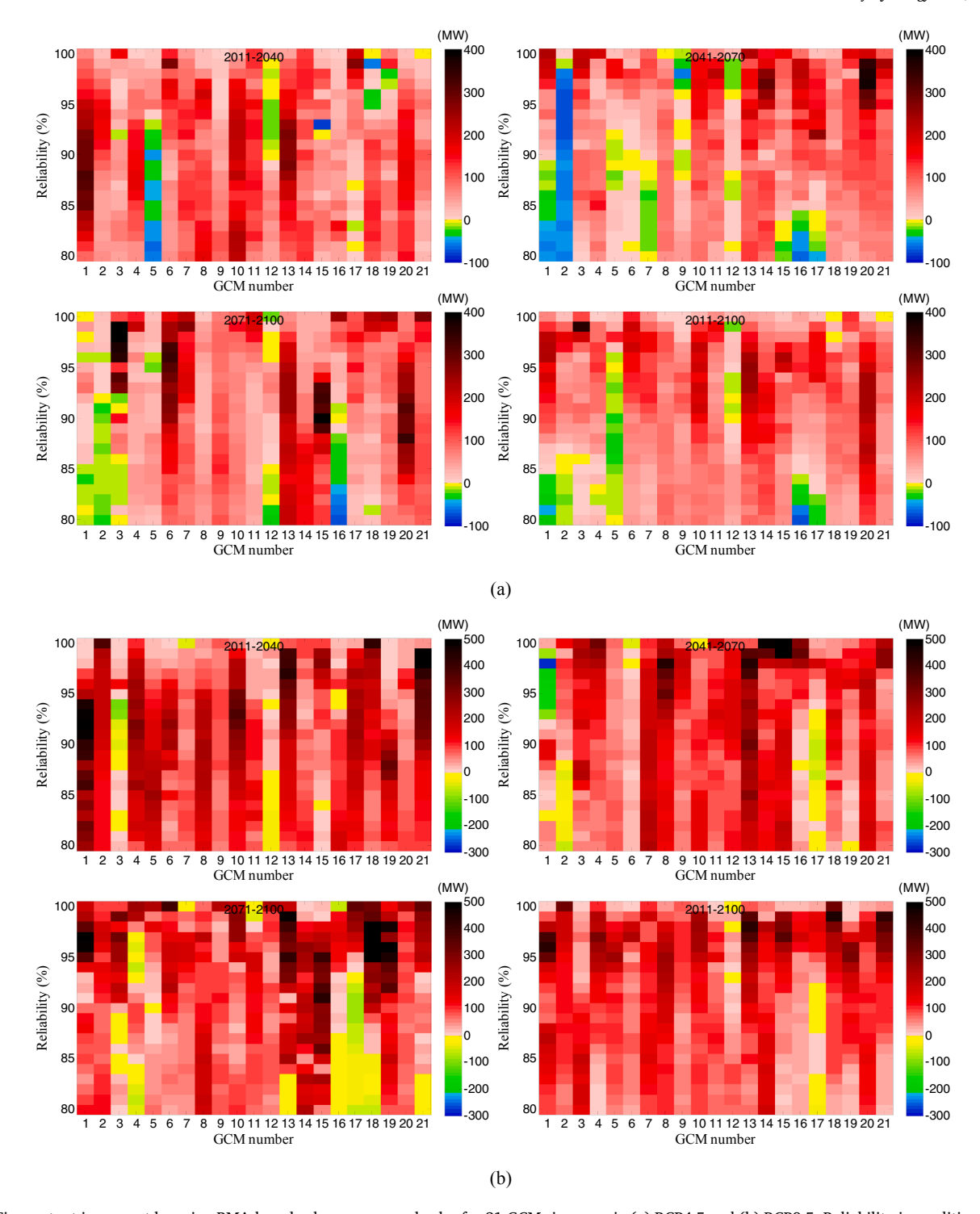


Fig. 10. Firm output increment by using BMA-based rules over normal rules for 21 GCMs in scenario (a) RCP4.5 and (b) RCP8.5. Reliability is conditioned on each GCM time-series individually; a 95% reliability implies that a power output threshold is met or exceeded in 95% of the months during the given period for that GCM.

can outperform conventional adaptive rules in terms of total power generation and firm power output simultaneously for some GCMs (such as GCM10 under RCP4.5 and GCM8 under RCP8.5), overall the Bayesian adaptive rules do not consistently provide superior performance.

Given that streamflow non-stationarity may be attributed to many factors (e.g. emission of greenhouse gases, changes in catchment characteristics) it is challenging to accurately identify all non-stationary components and incorporate them into water resources management. The findings in this paper not only illustrate the effectiveness of the proposed Bayesian adaptive framework but also reveal the possibility of

tackling adaptive water resources operation problems in the future from the perspective of time and frequency domains. In that way, the non-stationary features in streamflow at multiple time scales can be recognized with the support of time–frequency analysis and incorporated into water resources decision making. Future research efforts could focus on expanding and improving non-stationarity source detection and considering broader envelops of uncertainty (e.g., future water demand) in reservoir operation.

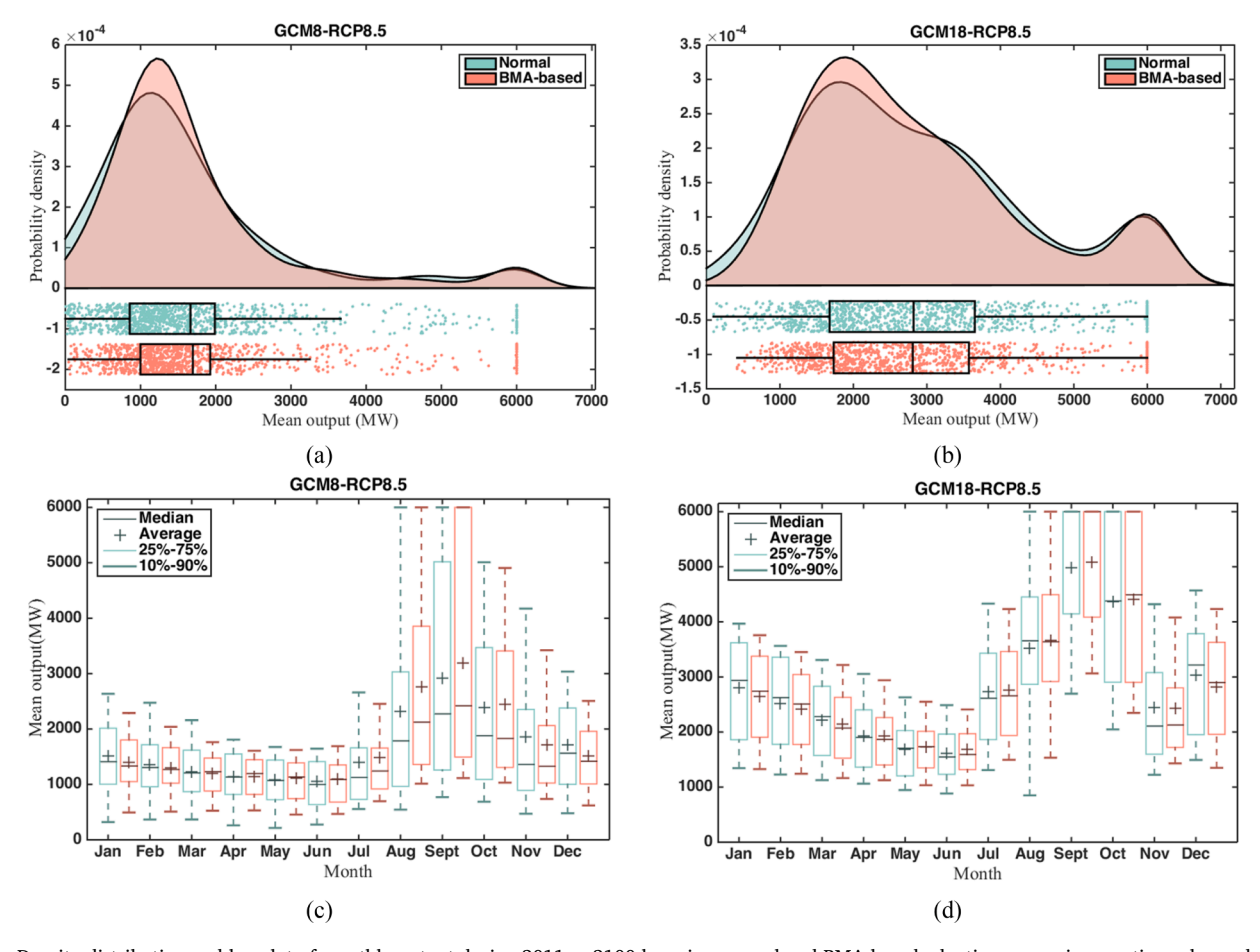


Fig. 11. Density distribution and boxplot of monthly output during $2011 \sim 2100$ by using normal and BMA-based adaptive reservoir operating rules under GCM8 and GCM18 in scenario RCP8.5. Green and red boxes refer to the results of normal and BMA-based rules. (For interpretation of the references to colour in this figure legend, the reader is referred to the web version of this article.)

Table 3Firm output increase (and percentage increase) of BMA-based rules (MW).

Scenarios	Reliability	Time periods (year)					
		2011 ~ 2040	2041 ~ 2070	2071 ~ 2100	2011 ~ 2100		
RCP4.5	80%	77 (9.5%)	25 (2.2%)	54 (5.1%)	39 (3.9%)		
	85%	96 (14.4%)	48 (4.8%)	72 (7.6%)	51 (5.9%)		
	90%	105 (20.1%)	60 (6.9%)	102 (13.1%)	83 (12%)		
	95%	95 (27%)	95 (14.4%)	93 (16.7%)	114 (25.7%)		
	100%	56 (50.2%)	102 (37.1%)	112 (66.8%)	41 (69.1%)		
RCP8.5	80%	93 (10.4%)	82 (6.4%)	53 (3.1%)	63 (5.4%)		
	85%	120 (16.1%)	78 (6.8%)	69 (4.6%)	87 (8.6%)		
	90%	154 (28.1%)	103 (10.4%)	89 (7.2%)	86 (10.1%)		
	95%	142 (39.5%)	103 (13%)	201 (24.4%)	159 (28.7%)		
	100%	70 (63.8%)	156 (56.8%)	164 (53.5%)	64 (129.4%)		

CRediT authorship contribution statement

Guang Yang: Methodology, Visualization. **Benjamin Zaitchik:** Funding acquisition, Investigation. **Hamada Badr:** Data curation, Resources. **Paul Block:** Conceptualization, Supervision.

Declaration of Competing Interest

The authors declare that they have no known competing financial interests or personal relationships that could have appeared to influence the work reported in this paper.

Acknowledgement

This work was partially supported by NSF INFEWS award 1639214.

Appendix A. Supplementary data

Supplementary data to this article can be found online at https://doi.org/10.1016/j.jhydrol.2021.125959.

References

Ahmadi, M., Haddad, O.B., Loáiciga, H.A., 2015. Adaptive reservoir operation rules under climatic change. Water Resour. Manag. 29 (4), 1247–1266.

Allcott, H., Collard-Wexler, A., O'Connell, S.D., 2016. How do electricity shortages affect industry? Evidence from India. Am. Fron. Rev. 106 (3), 587–624.

Allen, M.R., Ingram, W.J., 2002. Constraints on future changes in climate and the hydrologic cycle. Nature 419 (6903), 228.

Ashofteh, P.-S., Haddad, O.B., Loáiciga, H.A., 2015. Evaluation of climatic-change impacts on multiobjective reservoir operation with multiobjective genetic programming. J. Water Res. Plan. Man. 141 (11), 04015030.

Badr, H.S., Zaitchik, B.F., Guikema, S.D., 2014. Application of statistical models to the prediction of seasonal rainfall anomalies over the Sahel. J. Appl. Meteorol. Climatol. 53 (3), 614–636.

Block, P., Strzepek, K., 2010. Economic analysis of large-scale upstream river basin development on the Blue Nile in Ethiopia considering transient conditions, climate variability, and climate change. J. Water Res. Plan. Man. 136 (2), 156–166. Journal of Hydrology 594 (2021) 125959

Borgomeo, E., et al., 2014. Risk-based water resources planning: Incorporating probabilistic nonstationary climate uncertainties. Water Resour. Res. 50 (8), 6850–6873.

G. Yang et al.

- Brown, C.M., et al., 2015. The future of water resources systems analysis: toward a scientific framework for sustainable water management. Water Resour. Res. 51 (8), 6110–6124.
- Brown, C., Ghile, Y., Laverty, M., Li, K., 2012. Decision scaling: linking bottom-up vulnerability analysis with climate projections in the water sector. Water Resour. Res. 48 (9).
- Cancelliere, A., Giuliano, G., Ancarani, A., Rossi, G., 2002. A neural networks approach for deriving irrigation reservoir operating rules. Water Resour. Manag. 16 (1), 71–88
- Ceres, R.L., Forest, C.E., Keller, K., 2017. Understanding the detectability of potential changes to the 100-year peak storm surge. Clim. Change 145 (1–2), 221–235.
- Chang, J., Wang, X., Li, Y., Wang, Y., Zhang, H., 2018. Hydropower plant operation rules optimization response to climate change. Energy 160, 886–897.
- Chaves, P., Chang, F.-J., 2008. Intelligent reservoir operation system based on evolving artificial neural networks. Adv. Water Resour. 31 (6), 926–936.
- Cochran, W.T., et al., 1967. What is the fast Fourier transform? Proc. IEEE 55 (10), 1664–1674.
- Colominas, M.A., Schlotthauer, G., Torres, M.E., 2014. Improved complete ensemble EMD: a suitable tool for biomedical signal processing. Biomed. Signal Process. Control 14, 19–29.
- Conway, D., 2000. The climate and hydrology of the Upper Blue Nile River. Geogr. J. 166
- Culley, S., et al., 2016. A bottom-up approach to identifying the maximum operational adaptive capacity of water resource systems to a changing climate. Water Resour. Res. 52 (9), 6751–6768.
- Deisenroth, M.P., Neumann, G., Peters, J., 2013. A survey on policy search for robotics. Foundations and Trends®. Robotics 2 (1–2), 1–142.
- Dettinger, M., Cayan, D., McCabe, G., Marengo, J., 2000. Multiscale streamflow variability associated with El Niño/Southern Oscillation. In: Diaz, H.F., Markgraf, V. (Eds.), El Niño and the Southern Oscillation–Multiscale Variability and Global and Regional Impacts. Cambridge University Press, p. 113.
- Diks, C.G., Vrugi, J.A., 2010. Comparison of point forecast accuracy of model averaging methods in hydrologic applications. Stochastic Environ. Res. Risk Assess. 24 (6), 809–820.
- Duan, Q., Ajami, N.K., Gao, X., Sorooshian, S., 2007. Multi-model ensemble hydrologic prediction using Bayesian model averaging. Adv. Water Resour. 30 (5), 1371–1386.
- Ehsani, N., Vörösmarty, C.J., Fekete, B.M., Stakhiv, E.Z., 2017. Reservoir operations under climate change: storage capacity options to mitigate risk. J. Hydrol. 555, 435–446.
- Ek, M., et al., 2003. Implementation of Noah land surface model advances in the National Centers for Environmental Prediction operational mesoscale Eta model. J. Geophys. Res.: Atmos. 108 (D22).
- Eldaw, A.K., Salas, J.D., Garcia, L.A., 2003. Long-range forecasting of the Nile River flows using climatic forcing. J. Appl. Meteorol. 42 (7), 890–904.
- ETHIOPIA: Power Sector Market, 2016. Ethiopia Statistics. [Online], https://build.exp ort.gov/build/idcplg?IdcService=DOWNLOAD_PUBLIC_FILE&RevisionSelecti onMethod=Latest&dDocName=eg_us_tx_106929.
- Fletcher, S., Lickley, M., Strzepek, K., 2019. Learning about climate change uncertainty enables flexible water infrastructure planning. Nature Commun. 10 (1), 1–11.
- Funk, C., et al., 2015. The climate hazards infrared precipitation with stations—a new environmental record for monitoring extremes. Sci. Data 2, 150066.
- Gaudard, L., et al., 2014. Climate change impacts on hydropower in the Swiss and Italian Alps. Sci. Total Environ. 493, 1211–1221.
- Gelaro, R., et al., 2017. The modern-era retrospective analysis for research and applications, version 2 (MERRA-2). J. Clim. 30 (14), 5419–5454.
- Getirana, A.C., et al., 2012. The hydrological modeling and analysis platform (HyMAP): evaluation in the Amazon basin. J. Hydrometeorol. 13 (6), 1641–1665.
- Giuliani, M., Castelletti, A., Pianosi, F., Mason, E., Reed, P.M., 2015. Curses, tradeoffs, and scalable management: advancing evolutionary multiobjective direct policy search to improve water reservoir operations. J. Water Res. Plan. Man. 142 (2), 04015050.
- Giuliani, M., Anghileri, D., Castelletti, A., Vu, P.N., Soncini-Sessa, R., 2016. Large storage operations under climate change: expanding uncertainties and evolving tradeoffs. Environ. Res. Lett. 11 (3), 035009.
- Gleick, P.H., 2003. Global freshwater resources: soft-path solutions for the 21st century. Science 302 (5650), 1524–1528.
- Gosling, S.N., Arnell, N.W., 2016. A global assessment of the impact of climate change on water scarcity. Clim. Change 134 (3), 371–385.
- Haasnoot, M., Kwakkel, J.H., Walker, W.E., ter Maat, J., 2013. Dynamic adaptive policy pathways: a method for crafting robust decisions for a deeply uncertain world. Global Environ. Change 23 (2), 485–498.
- Herman, J.D., Giuliani, M., 2018. Policy tree optimization for threshold-based water resources management over multiple timescales. Environ. Modell. Softw. 99, 39–51.
- Herman, J.D., Reed, P.M., Zeff, H.B., Characklis, G.W., 2015. How should robustness be defined for water systems planning under change? J. Water Res. Plan. Man. 141 (10), 04015012.
- Herman, J.D., Quinn, J.D., Steinschneider, S., Giuliani, M., Fletcher, S., 2019. Climate adaptation as a control problem: review and perspectives on dynamic water resources planning under uncertainty. Water Resour. Res. e24389.
- Hoeting, J.A., Madigan, D., Raftery, A.E., Volinsky, C.T., 1999. Bayesian model averaging: a tutorial. Statistical Sci. 382–401.

Huang, N.E., et al., 1998. The empirical mode decomposition and the Hilbert spectrum for nonlinear and non-stationary time series analysis. Proc. R. Soc. London A 903–995

- Huang, H., et al., 2019. Combination of multiple data-driven models for long-term monthly runoff predictions based on Bayesian model averaging. Water Resour. Manag. 33 (9), 3321–3338.
- Huang, N.E., Wu, Z., 2008. A review on Hilbert-Huang transform: method and its applications to geophysical studies. Rev. Geophys. 46 (2).
- Hyndman, R.J., Khandakar, Y., 2007. Automatic Time Series for Forecasting: The Forecast Package for R. Monash University, Department of Econometrics and Business Statistics
- Jameel, A.L., 2014. The Grand Ethiopian Renaissance Dam: An Opportunity for Collaboration and Shared Benefits in the Eastern Nile Basin. World Water and Food Security Lab, Amicus Brief, pp. 1–17.
- Jeuland, M., Whittington, D., 2014. Water resources planning under climate change: assessing the robustness of real options for the Blue Nile. Water Resour. Res. 50 (3), 2086–2107
- Katz, R.W., Brown, B.G., 1992. Extreme events in a changing climate: variability is more important than averages. Clim. Change 21 (3), 289–302.
- King, A., Block, P., 2014. An assessment of reservoir filling policies for the Grand Ethiopian Renaissance Dam. J. Water Clim. Change 5 (2), 233.
- Koppa, A., Gebremichael, M., Zambon, R.C., Yeh, W.W.G., Hopson, T.M., 2019. Seasonal hydropower planning for data-scarce regions using multimodel ensemble forecasts, remote sensing data, and stochastic programming. Water Resour. Res. 55 (11), 8582, 8607
- Koutsoyiannis, D., Montanari, A., 2015. Negligent killing of scientific concepts: the stationarity case. Hydrol. Sci. J. 60 (7–8), 1174–1183.
- Kumar, S.V., et al., 2006. Land information system: an interoperable framework for high resolution land surface modeling. Environ. Modell. Softw. 21 (10), 1402–1415.
- Maier, H.R., et al., 2016. An uncertain future, deep uncertainty, scenarios, robustness and adaptation: how do they fit together? Environ. Modell. Softw. 81, 154–164
- McCabe, G.J., Betancourt, J.L., Hidalgo, H.G., 2007. Associations of decadal to multidecadal sea-surface temperature variability with Upper Colorado River Flow 1. JAWRA J. Am. Water Resour. Assoc. 43 (1), 183–192.
- Milly, P.C.D., et al., 2008. Stationarity is dead: whither water management? Science 319 (5863), 573–574.
- Milly, P.C., Dunne, K.A., Vecchia, A.V., 2005. Global pattern of trends in streamflow and water availability in a changing climate. Nature 438 (7066), 347.
- Moss, R.H., et al., 2010. The next generation of scenarios for climate change research and assessment. Nature 463 (7282), 747.
- Nalley, D., Adamowski, J., Khalil, B., Biswas, A., 2016. Inter-annual to inter-decadal streamflow variability in Quebec and Ontario in relation to dominant large-scale climate indices. J Hydrol. 536, 426–446.
- Nash, J., 1970. River flow forecasting through conceptual models, I: a discussion of principles. J Hydrol. 10, 398–409.
- National Planning Commission, 2016. Growth and transformation plan ii (GTP II)(2015/16-2019/20). Addis Ababa: Federal Democratic Republic of Ethiopia.
- Ngo, L.A., Masih, I., Jiang, Y., Douven, W., 2018. Impact of reservoir operation and climate change on the hydrological regime of the Sesan and Srepok Rivers in the Lower Mekong Basin. Clim. Change 149 (1), 107–119.
- Nile Basin Initiative, 2012. State of the River Nile basin. Entebbe (Uganda): Nile Basin Initiative Secretariat.
- Nowak, K., Hoerling, M., Rajagopalan, B., Zagona, E., 2012. Colorado River basin hydroclimatic variability. J. Clim. 25 (12), 4389–4403.
- Poff, N.L., et al., 2016. Sustainable water management under future uncertainty with eco-engineering decision scaling. Nature Clim. Change 6 (1), 25.
- Raso, L., Kwakkel, J., Timmermans, J., Panthou, G., 2019. How to evaluate a monitoring system for adaptive policies: criteria for signposts selection and their model-based evaluation. Clim. Change 153 (1–2), 267–283.
- Rathinasamy, M., Adamowski, J., Khosa, R., 2013. Multiscale streamflow forecasting using a new Bayesian Model Average based ensemble multi-wavelet Volterra nonlinear method. J. Hydrol. 507, 186–200.
- Robinson, B., Herman, J.D., 2019. A framework for testing dynamic classification of vulnerable scenarios in ensemble water supply projections. Clim. Change 152 (3–4), 431–448.
- Soltani, F., Kerachian, R., Shirangi, E., 2010. Developing operating rules for reservoirs considering the water quality issues: application of ANFIS-based surrogate models. Expert Syst. Appl. 37 (9), 6639–6645.
- Steinschneider, S., Brown, C., 2012. Dynamic reservoir management with real-option risk hedging as a robust adaptation to nonstationary climate. Water Resour. Res. 48 (5).
- Taye, M.T., Willems, P., 2012. Temporal variability of hydroclimatic extremes in the Blue Nile basin. Water Resour. Res. 48 (3).
- Taylor, K.E., Stouffer, R.J., Meehl, G.A., 2012. An overview of CMIP5 and the experiment design. Bull. Am. Meteorol. Soc. 93 (4), 485–498.
- Tesfa, B., 2013. Benefit of grand Ethiopian renaissance dam project (GERDP) for Sudan and Egypt.
- Thorarinsdottir, T., Guttorp, P., Drews, M., Kaspersen, P.S., de Bruin, K., 2017. Sea level adaptation decisions under uncertainty. Water Resour. Res. 53 (10), 8147–8163.
- Thrasher, B., et al., 2013. Downscaled climate projections suitable for resource management. Eos, Trans. Am. Geophys. Union 94 (37), 321–323.
- Tolson, B.A., Shoemaker, C.A., 2007. Dynamically dimensioned search algorithm for computationally efficient watershed model calibration. Water Resour. Res. 43 (1).
 Torrence, C., Compo, G.P., 1998. A practical guide to wavelet analysis. Bull. Am. Meteorol. Soc. 79 (1), 61–78.

- Walsh, C.L., et al., 2016. Adaptation of water resource systems to an uncertain future. Hydrol. Earth Syst. Sci. 20 (5), 1869–1884.
- Wu, Z., Huang, N.E., 2004. A study of the characteristics of white noise using the empirical mode decomposition method. Proc. R. Soc. London A 1597–1611.
- Wu, Z., Huang, N.E., Long, S.R., Peng, C.-K., 2007. On the trend, detrending, and variability of nonlinear and nonstationary time series. Proc. Natl. Acad. Sci. 104 (38), 14889–14894.
- Wu, Z., Huang, N.E., 2009. Ensemble empirical mode decomposition: a noise-assisted data analysis method. Adv. Adaptive Data Anal. 1 (01), 1–41.
- WWAP, 2019. The United Nations world water development report 2019: leaving no one behind. The United Nations world water development report 2019: leaving no one behind. Paris, UNESCO.
- Xiong, F., et al., 2019. A general framework of design flood estimation for cascade reservoirs in operation period. J. Hydrol. 577, 124003.
- Xu, W., Zhao, J., Zhao, T., Wang, Z., 2014. Adaptive reservoir operation model incorporating nonstationary inflow prediction. J. Water Res. Plan. Man. 141 (8), 04014099.

- Yang, T., Gao, X., Sorooshian, S., Li, X., 2016. Simulating California reservoir operation using the classification and regression-tree algorithm combined with a shuffled cross-validation scheme. Water Resour. Res. 52 (3), 1626–1651.
- Yang, T., Liu, X., Wang, L., Bai, P., Li, J., 2020. Simulating hydropower discharge using multiple decision tree methods and a dynamical model merging technique. J. Water Res. Plan. Man. 146 (2), 04019072.
- Yang, P., Ng, T.L., 2017. Fuzzy inference system for robust rule-based reservoir operation under nonstationary inflows. J. Water Res. Plan. Man. 143 (4), 04016084.
- Zaroug, M.A., Eltahir, E.A., Giorgi, F., 2014. Droughts and floods over the upper catchment of the Blue Nile and their connections to the timing of El Niño and La Niña events. Hydrol. Earth Syst. Sci. 18 (3), 1239–1249.
- Zhang, J., Liu, P., Wang, H., Lei, X., Zhou, Y., 2015. A Bayesian model averaging method for the derivation of reservoir operating rules. J. Hydrol. 528, 276–285.
- Zhang, X., Srinivasan, R., Bosch, D., 2009. Calibration and uncertainty analysis of the SWAT model using Genetic Algorithms and Bayesian Model Averaging. J Hydrol. 374 (3–4), 307–317.